

The stellar population and complex structure of the bright-rimmed cloud IC 1396N

M. T. Beltrán¹, F. Massi², R. López³, J. M. Girart⁴, and R. Estalella³

¹ Universitat de Barcelona, Departament d'Astronomia i Meteorologia, Unitat Associada a CSIC, Martí i Franquès 1, 08028 Barcelona, Catalunya, Spain

² INAF-Osservatorio Astrofisico di Arcetri, Largo E. Fermi 5, 50125 Firenze, Italy

³ Departament d'Astronomia i Meteorologia, Universitat de Barcelona, Martí i Franquès 1, 08028 Barcelona, Catalunya, Spain

⁴ Institut de Ciències de l'Espai (CSIC-IEEC), Campus UAB, Facultat de Ciències, Torre C-5, 08193, Bellaterra, Catalunya, Spain

Received date; accepted date

ABSTRACT

Context. IC 1396N is a bright-rimmed cloud associated with an intermediate-mass star-forming region, where a number of Herbig-Haro objects, H₂ jet-like features, CO molecular outflows, and millimeter compact sources have been observed.

Aims. To study in detail the complex structure of the IC 1396N core and the molecular outflows detected in the region and to reveal the presence of additional YSOs inside this globule.

Methods. We carried out a deep survey of the IC 1396N region in the *J, H, K'* broadband filters and deep high-angular resolution observations in the H₂ narrowband filter with NICS at the TNG telescope. The completeness limits in the 2MASS standard are $K_s \sim 17.5$, $H \sim 18.5$ and $J \sim 19.5$.

Results. A total of 736 sources have been detected in all three bands within the area where the *JHK'* images overlap. There are 128 sources detected only in *HK'*, 67 detected only in *K'*, and 79 detected only in *JH*. We found only few objects exhibiting a Near-Infrared excess and no clear signs of clustering of sources towards the southern rim. In case of triggered star formation in the southern rim of the globule, this could be very recent, because it is not evidenced through Near-Infrared imaging alone. The H₂ emission is complex and knotty and shows a large number of molecular hydrogen features spread over the region, testifying a recent star-formation activity throughout the whole globule. This emission is resolved into several chains or groups of knots that sometimes show a jet-like morphology. The shocked clowdlet model scenario previously proposed to explain the V-shaped morphology of the CO molecular outflow powered by the intermediate-mass YSO BIMA 2 seems to be confirmed by the presence of H₂ emission at the position of the deflecting western clump. New possible flows have been discovered in the globule, and some of them could be very long. In particular, the YSO BIMA 3 could be powering an old and poor collimated outflow.

Key words. ISM: individual objects: IC 1396N, IRAS 21391+5802 – ISM: jets and outflows – ISM: lines and bands – infrared: ISM – stars: formation

1. Introduction

Bright-rimmed clouds (BRCs) found in H_{II} regions are potential sites of triggered star formation due to compression by ionization/shock fronts. Many of them are associated with IRAS point sources with cold color indices (low dust temperature), which are most probably Young Stellar Objects (YSOs) or protostars. Such clouds are of deep interest from the point of view of ongoing star formation. They frequently contain a small cluster of Near-Infrared (NIR) stars that is elongated toward the bright-rim tip or the ionizing star(s) of the H_{II} region with the IRAS sources situated near the other end. There is a tendency for bluer (i.e., older) stars to be located closer to the ionizing star(s), and for redder (i.e., younger) stars to be closer to the IRAS sources. This asymmetric distribution of the cluster members strongly suggests small-scale sequential star formation or propagation of star formation from the side of the ionizing star(s) to the IRAS position in a few times 10^5 yr, as a result of the advance of the shock caused by the UV radiation from the ionizing star(s) (Sugitani et al. 1995). Thus, BRCs represent one of the best laboratories for studying the star-formation process at different evolutionary stages.

A good example of BRC with ongoing star-formation activity is IC 1396N (BRC38; Sugitani et al. 1991), located in the Cep OB2 association at a distance of 750 pc (Matthews 1979), and exposed to UV radiation from the O6.5 star HD 206267. The region is associated with IRAS 21391+5802, a very young intermediate-mass object with a luminosity of $235 L_\odot$ (Saraceno et al. 1996), which is powering an extended CO bipolar outflow (Sugitani et al. 1989). Beltrán et al. (2002) have resolved the millimeter emission towards IRAS 21391+5802 into an intermediate-mass source named BIMA 2 surrounded by two less massive and smaller objects, BIMA 1 and BIMA 3. Recent higher angular resolution millimeter interferometric observations have revealed that the intermediate-mass protostar BIMA 2 consists in fact of multiple compact sources (Neri et al. 2007). The gas emission surrounding IRAS 21391+5802 traces different molecular outflows (Codella et al. 2001; Beltrán et al. 2002, 2004), some of them possibly being powered by yet undetected YSOs (Beltrán et al. 2004). Beltrán et al. (2002) have conducted a detailed study of the bipolar outflow associated with the intermediate-mass protostar BIMA 2, and shown that its complex morphology and kinematics are possibly the result of the interaction between the outflow and the dense cores surrounding the protostar. NIR images of the region have also revealed

the presence of a number of small scale molecular hydrogen and Herbig-Haro (HH) flows (Nisini et al. 2001; Sugitani et al. 2002a; Reipurth et al. 2003; Caratti o Garatti et al. 2006). This evidence for ongoing star-formation activity at the head of the cometary globule together with the relatively proximity of the region make IC 1396N one of the best candidates to study potential sequential star formation.

To do a complete and uniform census of the young stellar population in the globule and reveal the presence of additional young sources inside the globule, deep NIR observations at J , H and K' have been carried out. In addition, deep high angular resolution observations in the S(1) $v=1-0$ line of H_2 at $2.12\ \mu m$ have also been performed to investigate the complex structure of this globule, and the morphology of the shocked gas that traces the interaction between the outflows in the region and the dense clumps surrounding the YSOs. The results of this NIR study are presented here.

2. Observations and data reduction

The images were taken with NICS (Baffa et al. 2001) at the 3.58-m Telescopio Nazionale Galileo (TNG) telescope (ORM, La Palma, Spain) through the standard J , H , K' broadband filters and the H_2 narrowband filter centered at $2.12\ \mu m$, during the nights between 16–17 July 2005. The plate scale is $0.25''/\text{pixel}$, yielding a field of view of $\sim 4.2 \times 4.2\ \text{arcmin}^2$. Both in K' and in H_2 , two positions roughly $100''$ apart (east-west) were imaged, such as to have an overlapping field, $\sim 150''$ wide (in RA), enclosing the globule. In H , the two imaged positions are separated by $\sim 50''$ east-west, so the overlapping field is $\sim 200''$ wide. Due to shortage of time, only one field could be imaged in J , centered on the globule. The seeing was $\sim 0.8''$ in K' , H and H_2 , and $\sim 0.9''$ in J . In K' and H , groups of five on-source integrations with a dithering of up to $10''$ in RA and DEC were interspersed between groups of five off-source integrations. The off-source fields are located $\sim 6'$ from the target and had been chosen through examination of 2MASS images. The dithering of the off-source frames is up to $20''$ in RA and DEC. In J , groups of two on-source images were interspersed between groups of two off-source images. Ditherings and off-source fields are the same as above. Finally, in H_2 pairs of one on-source and one off-source images were taken, with the same ditherings and off-source fields as above. Each frame was integrated 5 or 10 s in K' , depending on the background level; the total integration time is 600 s for each of the two positions. At H , each individual integration is 20 s and the total integration time is 600 s for each of the two positions, as well. At J , each individual integration is 100 s and the total integration time is 600 s. In H_2 , the individual integration times are 100 or 150 s, depending on the background level, and the total integration time is 2700 s for each of the two positions.

Each frame was first corrected for cross-talk using the routine provided on the TNG web page (<http://www.tng.iac.es>). Data were then reduced in the standard way by using IRAF¹ routines. Flat-field frames were acquired at sunset. Differential flat-field images were constructed for K' and H_2 , whereas all available frames with roughly the same mean level of counts were averaged together for H and J . All on-source and off-source frames were then flat-field corrected. Sky frames were constructed by

median-averaging the six off-source frames closest to each on-source frame (generally, three preceding and three following), after removal of the imaged stars. The sky frames were then subtracted from the corresponding on-source frames. At K' and H_2 , the sky-subtracted images were multiplied by a factor when obtained with different individual exposure times, such as to “convert” the counts of all frames in a same band to a same exposure time. After bad-pixel correction, all images in a same band were registered and combined together by using a median filter. The composite three color JHK' image of the area where the JHK' frames overlap is shown in Fig. 1.

Photometry on all mosaiced images was performed by using DAOPHOT (in IRAF). The detected stars were retrieved by running DAOFLIND and, subsequently, by a visual check in order to discard fake detections and add undetected faint sources. Aperture photometry was carried out through PHOT, by adopting an aperture $\sim 1FWHM$ in radius and an annulus $\sim 2FWHM$ wide with an inner radius $\sim 2FWHM$. The weather was barely photometric, so the calibration was performed by cross-correlating the sources found in the JHK' bands and the 2MASS point source catalog. A linear relation in the $J-H$ or $H-K'$ instrumental colors was fitted to the found pairs of instrumental magnitude and 2MASS magnitude and the corresponding instrumental color. Hence, the given magnitudes are in the 2MASS system (JHK_s). The color coefficient is always less than 0.06 in each band. As a check for consistency, we compared our K_s photometry and that of Nisini et al. (2001) for the isolated sources out of those listed by those authors. Our K_s values are on average 0.34 ± 0.28 mag dimmer than those by Nisini et al. (2001). This is very likely due to the much worse seeing ($\sim 2-3''$) and the much coarser sampling ($\sim 1''$) of the PSF in the data reported by Nisini et al. (2001), given the highly variable background level in the region.

Additional photometry of the detected H_2 features was performed from the narrowband H_2 image. The H_2 filter is centered at the $2.12\ \mu m$ line of molecular hydrogen. Continuum emission falls within the bandpass, as well as line emission. Through photometry in H_2 and K' , we estimated the fraction of stellar continuum affecting the total counts in the H_2 frame. First, based on the characteristics of the two filters, two scale factors can be derived by which we multiplied the H_2 and K' images, and then we subtracted the latter from the former. The resulting subtracted image contains only the line emission falling within the H_2 filter. The calibration was performed by carrying out stellar photometry on the H_2 original image, the same way as for JHK' but also including an aperture correction. The retrieved stars were cross-correlated with those found in the HK' bands and their correct flux was derived by interpolation with the corresponding ones at H and K_s in the 2MASS system. Through a fit, we determined the conversion factor from counts to flux. The detection limit (at a 3σ level) is $\sim 10^{-15}\ \text{erg cm}^{-2}\ \text{s}^{-1}\ \text{arcsec}^{-2}$. The procedure outlined above yielded an image where all stellar sources were efficiently removed, therefore only containing H_2 line emission knots. We classified each local emission peak as a knot and defined a polygon around each knot such as to include emission down to a $\sim 3\sigma$ limit. Polygon borders for close-by knots were chosen by eye, based on morphological criteria. Photometry was carried out by using POLYPHOT in IRAF.

The astrometric calibration was performed by deriving the positions of 14 relatively bright, isolated stars spread all over the K' frame, and correlating them with their 2MASS coordinates. By a fit (using STSDAS routines in IRAF) we obtained the transformation between frame and equatorial coordinates, allowing an accuracy of $\sim 1''$.

¹ IRAF is distributed by the National Optical Astronomy Observatories, which are operated by the Association of Universities for Research in Astronomy, Inc., under cooperative agreement with the National Science Foundation.

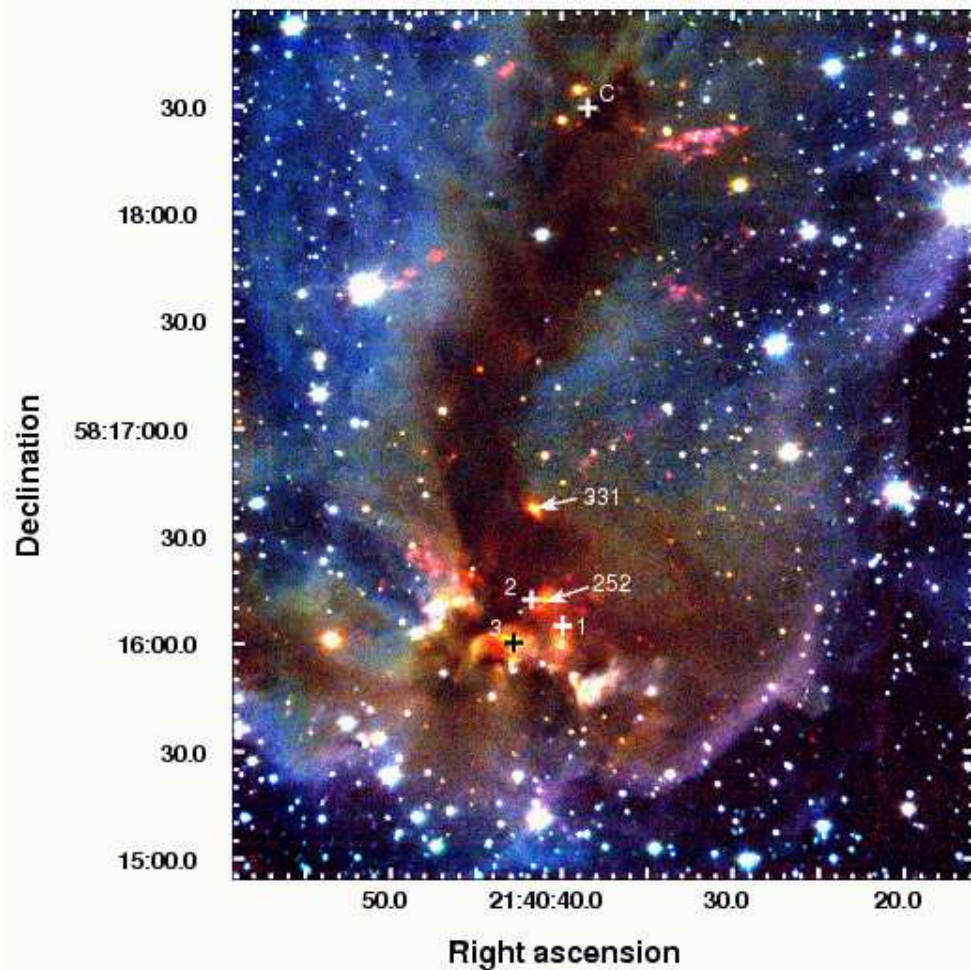


Fig. 1. Three color composite image of IC 1396N (J , blue, H , green, K' , red) taken with NICS at TNG. The black and white crosses show the positions of the 3.1 mm sources, BIMA 1, 2, and 3 from Beltrán et al. (2002), while the white cross in the top shows the position of the 1.3 mm continuum source C detected by Codella et al. (2001). Also labeled are two Class I sources discussed in the text.

3. Results and discussion

3.1. The stellar population

Within the area where the JHK' images overlap (see Fig. 1), we found 736 sources detected in all three bands, 128 sources detected only in HK' , 67 sources with a K' detection only, and 79 sources detected only in JH . The sources with HK' or K' detections only are preferentially located towards the globule (see, e. g. Fig. 4), as expected for heavily extinguished stars. Conversely, the sources with JH detections tend to be located outside the globule, indicating that these are just faint stars.

We obtained histograms of the number of sources as a function of magnitude by binning the number of sources detected in all three bands in magnitude intervals. Then, we adopted as completeness limit in each band the magnitude where the corresponding histogram peaks: $K_s \sim 17.5$, $H \sim 18.5$ and $J \sim 19.5$. When adding also the sources with detections in two or one bands only, the peak does not shift in any of the histograms but K_s , where it appears to move towards $K_s \sim 18$. The derived completeness limits are roughly 1.5 mag below our detection limits (at a 3σ level). An estimate of the minimum stellar mass detectable all over the globule can be obtained by using pre-main sequence (PMS) evolutionary tracks. However, one has to assume an age and a maximum extinction for the stellar popula-

tion. As for the age, Lada & Lada (2003) noted that the embedded phase of star cluster evolution lasts 2–3 Myrs and clusters older than 5 Myrs are rarely associated with molecular gas. This is in accord with the age of the open star cluster Trumpler 37, surrounding the globule ($\sim 3 \times 10^6$ yrs; Getman et al. 2007). The age of the star exciting the PDR around the globule may also give a hint of the age of the stellar population, since this star either triggered star formation in the core, or began inhibiting it by starting core destruction. If HD 206267 is an O6.5 V star (Walborn & Panek 1984), then its lifetime in the main sequence is $\sim 6 \times 10^6$ yrs (e. g. Vanbeveren et al. 1998), that roughly agrees with the times given above. On the other hand, the globule shows clear signature of much younger stars and protostars, and the dynamical timescales estimated from the jets (see Sect. 3.3) are even shorter, $\sim 10^3$ yrs. We can therefore assume an age of 10^6 yrs as a sort of upper limit, since younger low-mass PMS stars are brighter and, then, more easily detectable (lowering the mass detection limit). As for the maximum extinction, Getman et al. (2007) quote a few authors to conclude that the absorption through the core is $A_V \sim 9$ – 10 mag. Figures 2 and 3 clearly show that this value is probably too low and most of the detected stars exhibit $A_V \leq 20$ mag. Nevertheless, there are a few sources with A_V up to ~ 30 mag. More extinguished sources could be not represented in the diagrams just because too faint, thus biasing any

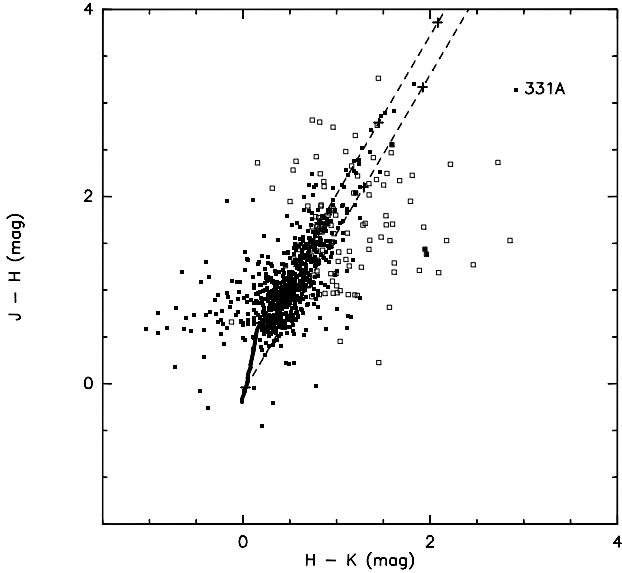


Fig. 2. Color-color diagram of the NIR sources found within the area where JHK' images overlap. Full squares are sources with detection in all bands, empty squares are sources with detection in HK_s only (hence, the shown $J-H$ is a lower limit). The solid line marks the main sequence (in the 2MASS system), the dashed lines follow the reddening law by Rieke & Lebofsky (1985) with crosses at intervals of $A_v = 10$ mag.

estimates based on the plots. In fact, towards BIMA 2, we can derive an extinction much larger than 100 mag from the continuum millimeter data. However, this is clearly a less evolved, very young region amounting to a small fraction of the globule. We can probably assume that for most of the globule the extinction does not exceed a canonical $A_V \sim 30\text{--}40$ mag.

We adopted the PMS evolutionary tracks by Palla & Stahler (1999), along with the reddening law by Rieke & Lebofsky (1985). Hence, assuming an age of 10^6 yrs, PMS stars of $\sim 0.1 M_\odot$ are within the completeness limit at K_s for $A_V = 30$ mag and within the detection limit at K_s for $A_V = 40$ mag. The same for PMS stars of $\sim 0.4 M_\odot$ at H , whereas PMS stars of $\sim 0.8 M_\odot$ are within the detection limit at J for $A_V = 30$ mag and PMS stars of $\sim 2 M_\odot$ are within the completeness limit at J for $A_V = 30$ mag. However, these magnitudes refer to “naked” stars, i. e., stars without a circumstellar disk.

The color-color diagram (CCD; $J-H$ vs. $H-K_s$) of the NIR sources found within the area where JHK' images overlap is shown in Fig. 2. The main sequence locus is also drawn, by using the colors of Koornneef (1983) after conversion to the 2MASS system through the relations given by Carpenter (2001). The CCD is consistent with that shown in Nisini et al. (2001), in that most of the stars fall within the reddening band of the main sequence and almost all those exhibiting a NIR excess lie only slightly below the reddening band. The points spread around the main sequence with larger NIR excesses are mostly faint sources found at the edge of the images, then affected by large errors. However, our source # 331 (labeled in figure) actually exhibits a large NIR excess. This source coincides with source # 8 in Nisini et al. (2001) and HH777 IRS in Reipurth et al. (2003). According to the latter authors, this source could be binary because it seems to be powering two flows, a major HH flow that expands towards the southwest, labeled HH777 by Reipurth et al. (2003), and a northwestern flow labeled G by Nisini et al. (2001). The source is neatly elongated with respect to the PSF of a single

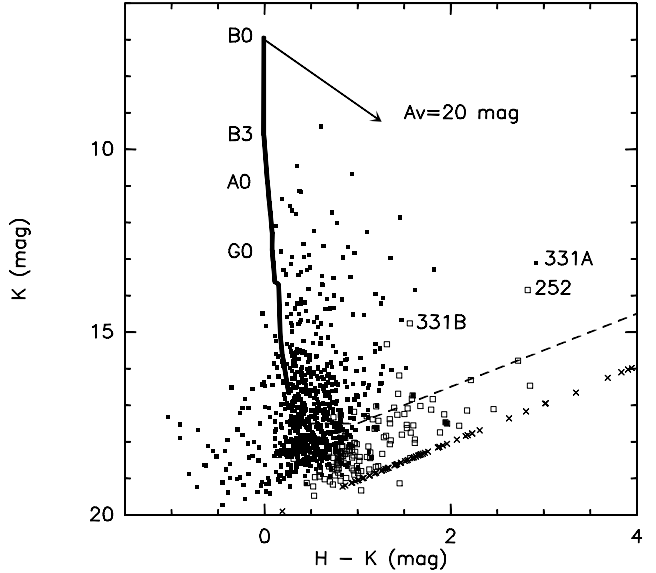


Fig. 3. Color-magnitude diagram of the NIR sources found towards the area where JHK' images overlap. Full squares are sources with detections in all bands, empty squares are sources with detections in HK_s only and crosses are sources detected at K_s only (hence, the shown $H-K_s$ is a lower limit). The solid line marks the zero age main sequence (from Allen (1976) and Koornneef (1983) after conversion to the 2MASS system) at a distance of 750 pc, the dashed lines indicate the completeness limit and an arrow is drawn showing a reddening $A_V = 20$ mag according to the reddening law by Rieke & Lebofsky (1985). A few spectral types on the ZAMS are labeled.

star, with the size of the major axis twice that of the minor axis, which suggests the binarity of the source. The nearby stars do not show such an elongation, therefore we discarded any possible focus effect. The elongation of source # 331 is very clear in the H filter, in which it has been possible to deconvolve the emission into two stars # 331A and # 331B by PSF-fit photometry with DAOPHOT in IRAF. In the K' filter the elongation is also evident, but the PSF-fit photometry appears to be less precise. Nevertheless, we cannot rule out the possibility that # 331B may be just radiation from # 331A scattered by dust through a cavity. This scenario would be consistent with the fact that the elongation of source # 331 roughly coincides with the direction of the southwestern HH777 flow (see Fig. 2 of Reipurth et al. 2003). However, as seen in Figs. 1 and 6, the other H_2 flow detected nearby, the northwestern flow labeled G, also points right back towards source # 331, which suggests that its powering source is also located at that position. Hence, based on the fact that there are two outflows associated with this position, we favor the scenario of binarity to explain the elongation of source # 331. The HK_s magnitude of # 331A is within 0.4 mag of those listed in the 2MASS catalog but, whereas its colors are consistent with those given by Nisini et al. (2001), the K_s value we derive is almost 1 mag larger than that measured by Nisini et al. (2001). This is still consistent with the difference found between the two photometries (see Sect. 2), also given that the source has been resolved into two close-by companions that appear to be embedded in a small diffuse nebulosity that probably could not be resolved by Nisini et al. (2001). However, a degree of intrinsic variability cannot be excluded, as well.

The color-magnitude diagram (CMD; $H-K_s$ vs. K_s) is shown in Fig. 3 for the NIR sources in the same area as above. As seen

in this diagram, an upper limit for the spectral type of the ZAMS stars in the cloud would be B1–B0, which corresponds to a stellar mass of $\sim 17\text{--}20 M_{\odot}$ (Vacca et al. 1996). Since such massive stars evolve along the ZAMS from $8\text{--}10 M_{\odot}$ on (e. g. Palla & Stahler 1991) at the end of their accretion phase, this can be considered as a robust upper limit for the mass of the stars associated with IC1396N, irrespective of their age. Most of the points lie within $A_V = 20$ mag of the zero age main sequence (ZAMS). However, source # 252 has similar K_s and $H-K_s$ as # 331A, both objects lying farther from the ZAMS than the remaining stellar population. Source # 252 is also embedded in a patch of diffuse nebulosity and is located near a cluster of H₂-emission blobs already identified by Nisini et al. (2001) as knot A, and the cluster of compact radio sources found by Beltrán et al. (2002). These facts suggest that sources # 252 and # 331A may be in a similar evolutionary stage, although this cannot be fully proved because # 252 has not been detected at J . They are located towards the center of the globule, $\sim 26''$ apart (see Fig. 1). Source # 252 lies close to the IRAS uncertainty ellipse, north-west of it. Projecting them back onto the ZAMS in the CMD, along the reddening vector, identify them as stars of spectral type B0 to B3. This has to be considered as a “lower” limit for their actual spectral type (i. e., they are of later spectral type), since # 331A exhibits a NIR excess and probably also # 252 does have it. Hence, based on the location of # 331A in the CCD, they might be Class I sources of intermediate mass (e.g. Sugitani et al. 2002b).

Getman et al. (2007) used CHANDRA X-ray observations of IC 1396N, complemented with Spitzer/IRAC photometry and the available NIR photometry, identifying 25 likely stellar members of the globule. Although all are associated with IRAC MIR sources, 6 of them do not have a NIR counterpart either in the 2MASS catalog or in the list of Nisini et al. (2001). We have found three new matches, e. g. sources 70, 76, and 80 (see Table 2 of Getman et al. (2007)), corresponding to our sources 224 ($K_s \sim 16$), 223 ($K_s \sim 16$) and 196 ($K_s \sim 17.7$), respectively. They are all undetected both in J and in H , confirming their nature of heavily extincted source. The remaining 3 X-ray sources without a NIR counterpart lie in the area of the BIMA sources and their X-ray spectra are heavily absorbed ($N_H \gtrsim 10^{23} \text{ cm}^{-1}$). One of them (source 66) has been proposed as X-ray counterpart of the protostar BIMA 2. However, note that our sources # 331A (and 331B) and 252 do not have an X-ray counterpart in the catalog of Getman et al. (2007). These authors quote a completeness limit (in mass) of $0.4 M_{\odot}$, higher than our completeness limit in K_s but similar to our completeness limit in H . We suspect that their completeness limit may be even higher, since the reddening towards the globule may be at least twice larger than adopted by them. It is noteworthy that Getman et al. (2007) found X-ray counterparts of possible Class I sources with high absorption and no NIR counterparts, but fail to detect our sources # 331A and 252. This would be consistent with # 331A and 252 being young intermediate-mass (proto-)stars. If # 331 is actually a double system, then its companion (possibly # 331B) might either be another young intermediate-mass star, or a low-mass protostar (with a mass below the X-ray completeness limit). Moreover, sensitive millimeter interferometric observations did not detect # 252 (Beltrán et al. 2002; Neri et al. 2007), which rules out the presence of the expected massive enough circumstellar disk. Hence, further data are needed to clarify its nature and its identification as an intermediate-mass Class I source remains highly speculative.

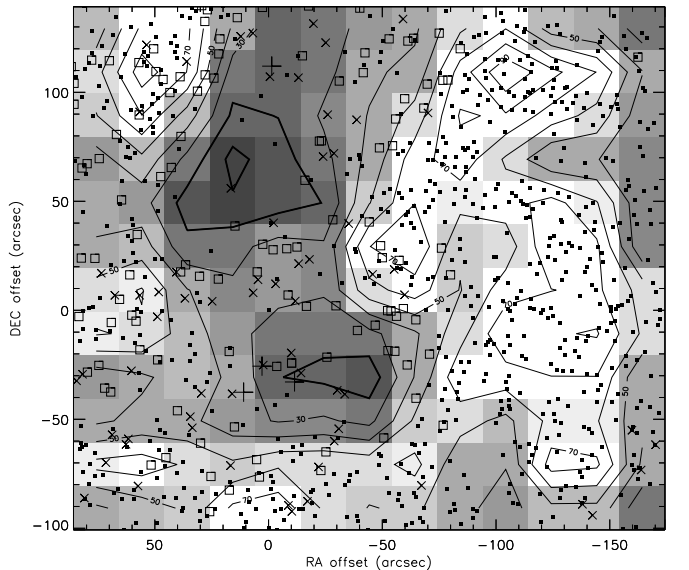


Fig. 4. Stellar surface density map (in stars arcmin⁻²) of all sources detected in the K_s band up to $K_s = 20$. Contours range from 10 to 90 stars arcmin⁻² in steps of 10 stars arcmin⁻². The contours at 10 and 20 stars arcmin⁻² are thicker. Grey scale ranges from -15 stars arcmin⁻² (black) to 69 stars arcmin⁻² (white). The field shown has been imaged at all bands and the offsets are in arcsec from the location of source # 331A (HH777 IRS). The positions of sources with detections in all bands are marked by filled squares, those of sources with detections at HK_s only by empty squares and those of sources with only a K_s detection are marked by small crosses. The three large crosses around $(0'', -30'')$ are the compact embedded sources BIMA 1, 2 and 3 detected by Beltrán et al. (2002) at millimeter wavelengths, and that at around $(0'', 110'')$ is the 1.3 mm continuum source C detected by Codella et al. (2001).

3.2. Triggered star formation?

In the X-ray source population towards IC 1396N, Getman et al. (2007) have found a clear clustering of sources at the southern rim, with an elongated spatial distribution, and an evolutionary gradient (interpreted as an age gradient), oriented towards the exciting star. These authors interpret this geometric and age distribution in terms of triggered star formation by passage of HII region shocks into the molecular globule. We have searched for evidence in the NIR of age gradients in the south-north direction or clustering of stars towards the rim, but found none. The number of sources with evidence of NIR excess towards the globule is too low, so any analysis of the stellar population in the NIR *alone* is bound to remain inconclusive with respect to the identification of age gradients. Regarding the geometric distribution of the sources in the NIR, there are no clear signs of clustering towards the rim (even within the area where X-ray sources cluster), as shown by the map of the star surface density (Fig. 4), which was obtained by counting all sources with a detection at least in the K_s band (up to $K_s = 20$) in squares of $40'' \times 40''$, displaced by $20''$ both in RA and in DEC. The number of sources decreases in going from the southern edge of the globule to the northern one; in the CCD, within the extinction band of the main sequence the upper and lower limits of extinction initially increase, then decrease close to the northern edge, as expected. What is more, the JHK_s sources lying below the main sequence reddening band in the CCD tend to cluster out

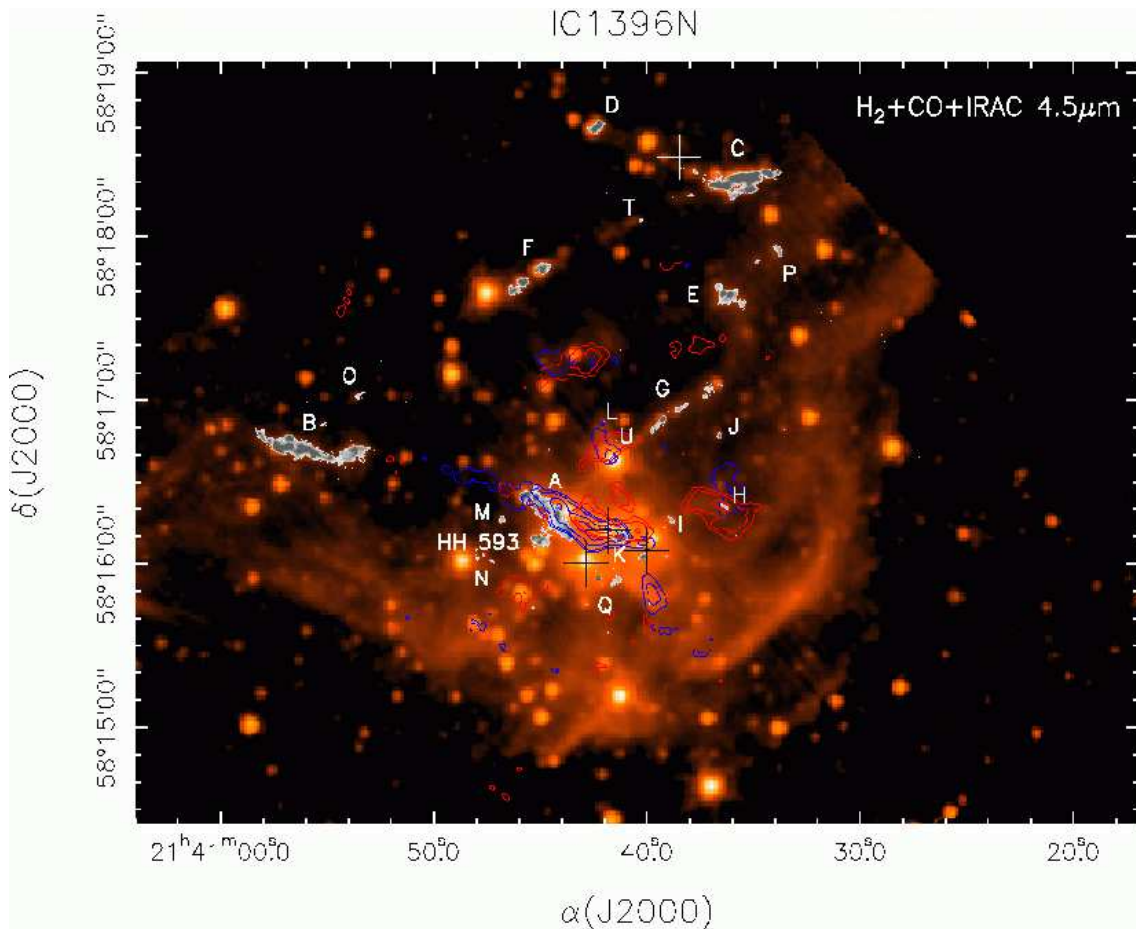


Fig. 5. H_2 (2.12 μm) image (continuum-subtracted) in grey-scale and CO ($J=1 \rightarrow 0$) emission in red and blue contours (Beltrán et al. 2002) overlaid with an IRAC 4.5 μm image. The H_2 emission shows a large number of molecular hydrogen features, many already found by Nisini et al. (2001), Reipurth et al. (2003), and Caratti o Garatti (2006), whose nomenclature we use and expand. The black crosses show the positions of the 3.1 mm sources, BIMA 1, 2, and 3 from Beltrán et al. (2002), and the white one shows the position of the 1.3 mm continuum source C detected by Codella et al. (2001).

of the eastern and western edge of the globule, but much less so towards the southern border. As discussed above, our JHK_s colors are biased towards unextincted PMS stars of all masses and heavily extinguished intermediate-mass young stars. Instead, HK_s colors only can evidence heavily extinguished PMS stars down to $0.4 M_\odot$. These appear to be mostly located towards the globule, but it is still difficult to evidence a significant clustering towards the southern border. A clearer clustering of reddened objects occurs towards the center of the globule. This is also visible as an increase of surface density (Fig. 4) north of sources # 331 (A and B), mostly due to sources with HK_s or K_s detection only.

Therefore, only very few or no sources with a NIR excess clusters towards the southern rim, as far as extinction is low and we are sensitive to very low masses. Of course, a number of stars with a NIR excess may concentrate north of the southern edge of the globule, towards the BIMA sources, were extinction is much higher. Then, any triggered YSOs may be still too young to be evidenced through NIR imaging alone. This would be consistent with the star surface density map (Fig. 4), which shows two surface density minima towards the globule, one in the southern part and one in the northern part. The southern one is close to the position of the embedded sources BIMA 1, BIMA 2, and BIMA 3 detected by Beltrán et al. (2002), and the northern one lies along the gas elongation visible in CO, CS (Codella et al. 2001) and H^{13}CO^+ (Sugitani et al. 2002a). These two surface density min-

ima outline the more extinguished (densest) parts of the globule, not yet visible at NIR wavelengths.

By decreasing the limiting magnitude to $K_s = 18$ (i. e., the completeness limit), one obtains a similar surface density map, but the “bridge” of sources crossing the two minima almost disappears, confirming it mostly arises from the detection of faint sources. If this were a real group of young stars associated with the globule, then their birth could hardly be explained as triggered, since they are located north of the group of the youngest protostars (the three compact radio sources found by Beltrán et al. 2002), farther from the ionization front. What is more, in going from south to north, one finds the cluster of Class 0/I sources observed at millimeter wavelengths by Beltrán et al. (2002) and Neri et al. (2007), then source # 331A, which is definitely a more evolved object, and then millimeter source C (Codella et al. 2001), which is a deeply embedded and very young object. Therefore, from the NIR and millimeter observations it is clear that not all the star formation in the globule can be explained in terms of triggering.

The difficulty in evidencing any stellar population associated with the globule based on NIR photometry only was already noted by Getman et al. (2007). As discussed, X-ray observations proved much more efficient in selecting this population, although clearly failing to probe all young stars and protostars. By combining X-ray and Spitzer/IRAC observations, they could indeed

find a number of Class I sources towards the globule. This confirms what we inferred from our NIR images. Also, those authors estimate that the total population of T Tauri stars of the globule is ~ 30 , also consistent with the lack of a significant increase in the NIR source surface density towards the rim. Nevertheless, the lack of sources exhibiting a clear NIR excess close to the rim is unusual for a stellar population of $\sim 10^6$ yrs old and strongly suggests that the intense UV radiation may have affected their circumstellar environments, suddenly stopping their growth. This would be confirmed by the low masses inferred for the counterparts of the X-ray sources associated with the globule. Most of them have estimated masses between $0.2\text{--}0.5 M_\odot$, and they would be even less massive if they were younger than 10^6 yrs, as assumed by Getman et al. (2007). Hence, we caution against interpreting an evolutionary gradient as an age gradient in an environment like the edge of a bright rimmed cloud. The eroding ionization front, in fact, may have dispersed the circumstellar environment of protostars downstream of it leaving them as naked stars, without significantly affect protostars upstream of it. In this case, an evolutionary gradient may not correspond to a real age gradient. As shown, star formation activity is present throughout the whole core, even in the northern part. Then, at the moment it appears really difficult proving that star formation in the southern rim has been triggered.

3.3. H_2 emission

Figure 5 shows the $2.12\ \mu\text{m}$ H_2 integrated line emission in grey-scale overlaid with an IRAC $4.5\ \mu\text{m}$ image in color obtained from the Spitzer Center Archive using the Leopard software. The title of the Spitzer program is *Star Formation in Bright Rimmed Clouds*, and the principal investigator is Giovanni Fazio. The CO ($J=1\rightarrow 0$) emission integrated in the low-velocity outflow interval $[\pm 3.5, \pm 9.5]\ \text{km s}^{-1}$ is also shown in red and blue contours (Beltrán et al. 2002). Figure 6 shows a close-up of the H_2 emission line features. As seen in these figures, the H_2 emission shows a large number of molecular hydrogen features spread over the region. Many of these emission features have already been found by Nisini et al. (2001), Reipurth et al. (2003), and Caratti o Garatti (2006). We have continued and expanded, when new H_2 features have been discovered, the nomenclature started by these authors (see Table 5). Most of the H_2 features are also visible in the IRAC $4.5\ \mu\text{m}$ image (Fig. 5). The fact that the IRAC $4.5\ \mu\text{m}$ band is very efficient in detecting Herbig-Haro object is due to the fact that the spectral response function is highest in this band, and that between $4\text{--}5\ \mu\text{m}$ there are many vibrational and rotational H_2 emission lines (see, e. g. Smith & Rosen 2005). In addition, the $4.5\ \mu\text{m}$ band is the less affected by polycyclic aromatic hydrocarbons (PAHs), whose emission could hide the shock excited H_2 features of the HH flows.

The H_2 emission is not smooth but complex and knotty, with several condensations embedded in a more diffuse and nebular emission (Fig. 6). The deep and sub-arcsecond resolution H_2 observations have allowed us to resolve the emission into several chains of knots that could be tracing different flows. Particularly interesting are the chains of knots labeled A, B, and C, for which more than 10 individual knots have been mapped. The peak position and photometry of the individuals knots are given in Table 5. We have named the individual components of the different H_2 emission line features by numbers. These chains or groups of H_2 knots show sometimes a jet-like morphology which together with the fact that are located in different parts of the globule, not just on the bright rim, suggests that the H_2 excitation is mostly

due to shocks driven by outflows powered by YSOs (Nisini et al. 2001).

3.3.1. H_2 knots and flows towards the BIMA sources.

Beltrán et al. (2002) observed the region surrounding the intermediate-mass YSO IRAS 21391+5802 (BIMA 2) in several molecular tracers and continuum at millimeter wavelengths with the BIMA interferometer. These authors resolved the millimeter continuum emission into three sources, BIMA 1, 2, and 3, and mapped in CO two molecular outflows: a north-south outflow powered by BIMA 1, and an east-west one driven by BIMA 2. The latter outflow shows a very complex morphology and kinematics because while at high outflow velocities the outflow is clearly bipolar, with the blueshifted emission towards the west and the redshifted one towards the east, at low outflow velocities the direction of the outflow gets deflected and the blueshifted and redshifted emission are highly overlapped (see Fig. 7). Beltrán et al. (2002) explain the complexity of this outflow in terms of a shocked clowdlet model scenario, in which the molecular outflow would interact with the dense material surrounding the embedded sources. The outflow is almost on the plane of the sky (Codella et al. (2001) assume an inclination angle of $10^\circ\text{--}20^\circ$), which would explain why the red- and blueshifted outflow emission overlap after the shock. In this section, we want to study in more detail the morphology of the BIMA 2 outflow and check the validity of the shocked scenario by comparing the $2.12\ \mu\text{m}$ H_2 emission with that of the outflow as seen in CO and CS with the BIMA interferometer. The top panel of Fig. 7 shows in red and blue contours the CO ($J=1\rightarrow 0$) emission integrated in the low-velocity outflow interval (Beltrán et al. 2002) overlapped on the $2.12\ \mu\text{m}$ H_2 integrated line emission in grey-scale. The angular resolution of this image is much higher than that of Fig. 5 of Nisini et al. (2001). What is more, the interferometer has filtered out the extended emission of the outflow allowing to better study the innermost part of the outflow and to compare the correlation between the H_2 and the CO emission. The bottom panels of Fig. 7 show a close-up image of the H_2 emission towards the embedded YSOs BIMA 1, 2, and 3, overlaid with the CO ($J=1\rightarrow 0$) emission integrated in the intermediate- (Fig. 7b), and high-velocity outflow interval (Fig. 7c), and the CS ($J=5\rightarrow 4$) integrated emission (Fig. 7d) of the BIMA 2 outflow in red and blue contours (Beltrán et al. 2002).

Figure 7c shows that at high outflow velocities, the CO outflow, which has a well-defined bipolar structure, stops before reaching the position of the H_2 emission. Interestingly, on the west side, the CO emission stops in front of the strong H_2 knots K1 and K2. The position of these two knots coincides with a blueshifted clump visible in CS ($J=5\rightarrow 4$) (Fig. 7d) and CH_3OH ($J=5\rightarrow 4$) and identified as clump B by Beltrán et al. (2002). These authors suggest that there is a shocked surface at the position of this clump, which would be the responsible of the deflection and V-shaped morphology of the molecular outflow at low and intermediate outflow velocities (Fig. 7a, b) westwards of BIMA 2. The detection of the H_2 knots K1 and K2 seems to confirm this scenario. Note that the knot K3, the strand of knots I, and the knot H1 are associated with the deflected CO emission (Fig. 7a, b). In particular, H1 is associated with a redshifted and blueshifted CO clump, also visible in CS ($J=2\rightarrow 1$) (Beltrán et al. 2002). Eastwards of BIMA 2, Beltrán et al. (2002) suggest that the redshifted clump visible in CS ($J=5\rightarrow 4$) (Fig. 7d) and CH_3OH ($J=5\rightarrow 4$) and named R is the responsible for the change in the velocity of the gas in the outflow. The eastern CO emission, between the driving source and clump R, is mainly red-

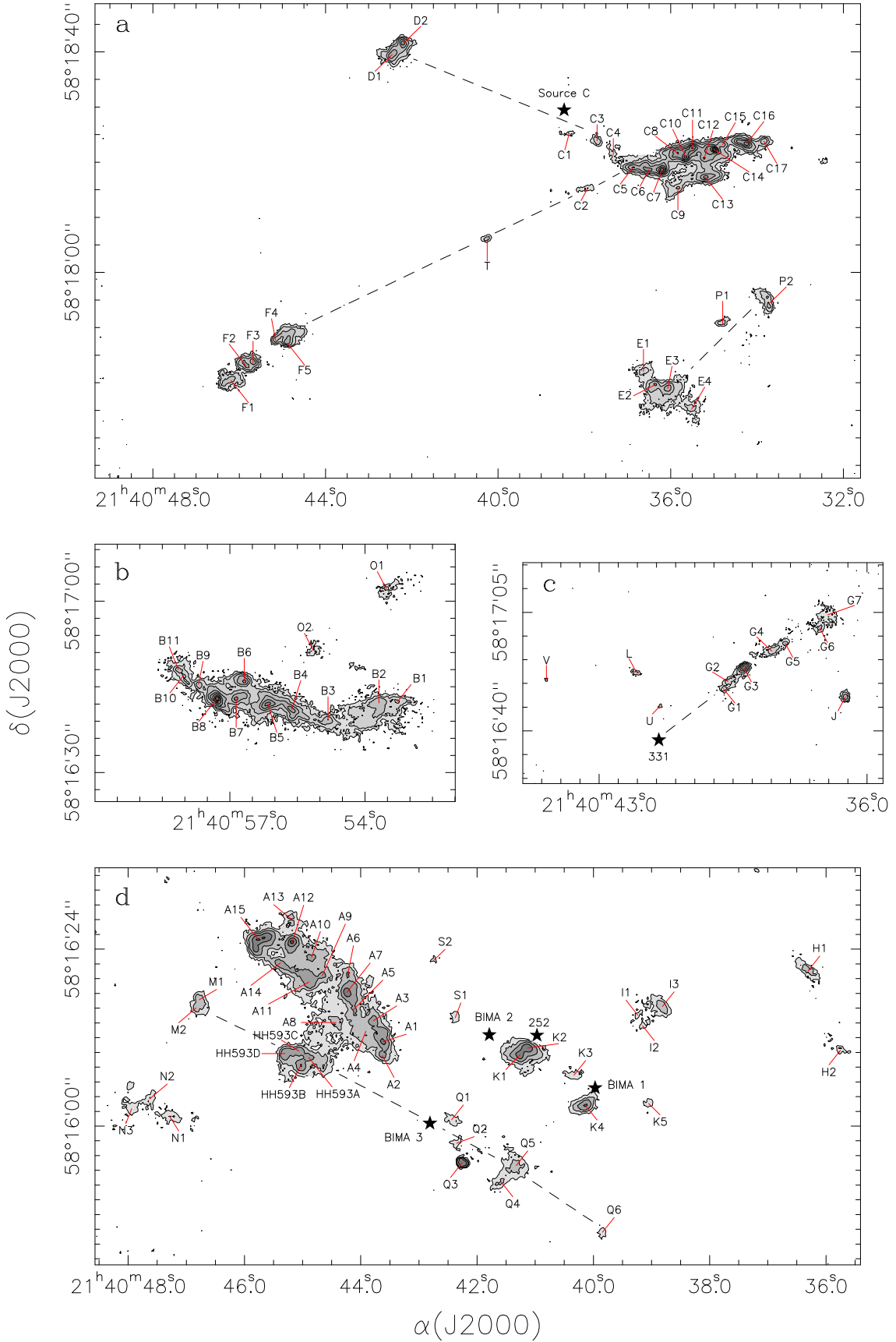


Fig. 6. H_2 ($2.12 \mu\text{m}$) close-up images (continuum-subtracted) of the resolved knots in the jet features towards IC 1396N, including the names of all the knots. The contours are in units of $5.7 \times 10^{-16} \text{ erg cm}^{-2} \text{ s}^{-1} \text{ arcsec}^{-2}$ (1, 2, 4, 8, 13, 20, 28 and 33). The black stars show the position of the 1.3 mm continuum source C detected by Codella et al. (2001) (top panel), of source # 331 (middle right panel), and of source # 252 and the 3.1 mm sources, BIMA 1, 2, and 3 detected by Beltrán et al. (2002) (bottom panel). The dashed lines indicate the orientation of the possible H_2 flows described in the text (see Sect. 3.3). Due to the complexity of the flow powered by BIMA 2 (see Sect. 3.3.1), its direction is not indicated.

shifted at intermediate and high outflow velocities, whereas farther away from clump R the outflow emission is slightly stronger in the blue wing than in the red wing. This clump R, however, is not visible in H₂ emission. A possible explanation for this could be that the H₂ molecules are dissociated in the shock, and thus, there is no enough H₂ to be detected. However, the most plausible explanation would be that the R clump, which is located towards the redshifted lobe of the outflow, is not visible in H₂ due to the extinction produced by the circumstellar material surrounding BIMA 2. Submillimeter observations carried out with the James Clerk Maxwell Telescope by Correia (2000) have estimated a circumstellar mass of $\sim 20 M_{\odot}$ associated with BIMA 2. There is indeed a small knot labeled S1 (Figs. 6d and 7d) in the red lobe side of the outflow. Although its position does not exactly coincide with that of the clump R, we cannot discard the possibility that this knot is part of the shell of the deflecting clump, where the extinction is lower. The H₂ emission is clearly detected farther east probably because the emission has shifted from redshifted to blueshifted and the H₂ flow has reached outside the core surrounding BIMA 2. In fact, the H₂ emission of the chain of knots A is clearly associated with the CO emission at low and intermediate outflow velocities (Fig. 7a, b). The knot labeled A15 (Fig. 6d), which is located at the tip of the chain of knots A is probably a bow-shock, as suggested by its curved morphology, and by its association with high-density gas as traced by CS ($J=5 \rightarrow 4$) and CS ($J=2 \rightarrow 1$) (Fig. 7 and Beltrán et al. 2002).

The CO emission extends farther out towards the east, in the direction of the chain of knots B. Unfortunately, this feature is located too far from the phase center of the millimeter observations, and therefore, the interferometer is not sensitive to the emission. In any case, Nisini et al. (2001) and Codella et al. (2001) show that there is CO emission also at the position of the strand of knots B. If the chain of knots A and B were both associated with the BIMA 2 outflow, then the length of this flow eastwards of BIMA 2 would be of ~ 2.3 or 0.5 pc at a distance of 750 pc, which corresponds to a dynamical timescale, t_{dyn} , of ~ 3300 yr for a typical jet velocity, v_{jet} , of 150 km s^{-1} (Reipurth & Bally 2001). Note, however, that to connect the intermediate-mass protostellar BIMA 2 with the knots in A and the knots in B, one cannot follow a straight line but a curved one (Fig. 7a). Such a curve is also visible in the CO emission and could suggest wiggling or precession of the flow. The precession of the BIMA 2 outflow could be possible if the powering source were a binary system instead. As a matter of fact, the intermediate-mass source BIMA 2 is not associated with a binary system but with a cluster, as recently reported by Neri et al. (2007), with at least 3 cores embedded inside a common envelope.

Regarding the other knots in the region, it is possible to trace a straight line to connect BIMA 3 with the group of knots labeled Q towards the southwest, and with the knots HH593 and the knots M1 and M2 towards the northeast. A dashed line in Fig. 6d indicates the possible direction of this flow. The straight line can be extrapolated up to reach the group of knots labeled B. In particular, the line can be traced towards knots B1 and B2 that have a different orientation from the rest of knots in B. This, together with the bow-shock shape of knots Q4 and Q5 (Fig. 6d), makes us to speculate with the possibility that BIMA 3 is driving an additional flow, which could have a length from BIMA 3 to B1 and B2 of ~ 1.6 or 0.35 pc, and $t_{\text{dyn}} \approx 2300$ yr for $v_{\text{jet}} = 150 \text{ km s}^{-1}$. The length of the flow from Q6 to M1 and M2 is ~ 1.1 or 0.24 pc. Although no CO ($J=1 \rightarrow 0$) emission has been detected towards the position of this possible outflow through interferometric observations (Fig. 7), Codella et al. (2001) have observed

CO ($J=2 \rightarrow 1$) through single-dish observations. Therefore, this could be an old and poor collimated outflow, whose emission has been filtered out by the interferometer.

No H₂ emission has been clearly found in association with the north-south outflow mapped in CO ($J=1 \rightarrow 0$) by Beltrán et al. (2002) and proposed to be driven by BIMA 1, nor with a possible additional CS ($J=2 \rightarrow 1$) outflow observed westwards of the BIMA 1 outflow (Beltrán et al. 2004).

3.3.2. Other possible H₂ flows in the globule

One of the H₂ features mapped in the region by Nisini et al. (2001) is the chain of knots labeled G. As seen in Fig. 6c, this strand of knots shows a jet-like morphology, with an elongation of $\sim 0.75'$ or ~ 0.16 pc. This possible flow seems to be emanating from source # 331, named HH777 IRS by Reipurth et al. (2003), which as discussed in Sect. 3.1 is possibly binary. One of the sources in this binary system could be driving the HH777 flow mapped by Reipurth et al. (2003). The HH777 flow has a PA of about -120° . This flow is visible in H_a and [SII] as a bright working surface abruptly emerging from the southwestern sharp rim of the cloud core (Reipurth et al. 2003). The bow-shock is also visible in the Digital Sky Survey 2 optical image (see Fig. 1 of Beltrán et al. 2002). Our H₂ observations do not cover the position of this bow-shock. As for the HH777 flow before emerging from the rim, that is, closer to source # 331, no H₂ emission has been detected. Regarding the chain of knots G, it is not easily associated with any of the CO ($J=2 \rightarrow 1$) peaks mapped by Codella et al. (2001), although it is clearly located in a region of enhanced high-velocity CO emission (see Fig. 5 of Nisini et al. 2001). No CO ($J=1 \rightarrow 0$) emission is detected either in association with the G knots in the interferometric maps of Beltrán et al. (2002) (see Fig. 5). This could be due to the fact that this feature is located too far from the phase center of the millimeter observations, and therefore, the interferometer is not sensitive to the emission. Small blueshifted and redshifted CO emission clumps have been detected towards the position of # 331 (Fig. 5), and Caratti o Garatti et al. (2006) have detected [FeII] as well. The dynamical timescale of the possible G flow would be of ~ 1000 yr for a typical v_{jet} . Interestingly, the strand of knots G points towards a northwestern cavity clearly visible in the IRAC 3.6, 4.5, 5.8, and $8.0 \mu\text{m}$ images, which makes us to speculate with the possibility that such a cavity has been excavated by a molecular outflow that could be associated with these H₂ knots.

Towards the north of the IC 1396N globule there are some other prominent groups or chains of knots, labeled C, D, E, F, and P. Nisini et al. (2001) propose that the strands of knots E and F could be associated with a flow, which they called outflow II, and that the chains of knots C and D could be associated with the two lobes of a same flow, called outflow III. In the latter scenario, the powering source of the possible C–D flow would be the 1.3 mm continuum source C detected by Codella et al. (2001) and visible in the top panel of Fig. 6. However, as seen in Fig. 6a, the group of knots E seems to be more likely associated with those labeled P, with the knot P2 showing a sort of bow-shock morphology. A dashed line in Fig. 6a indicates the possible direction of this flow. Regarding the flow C–D, there are some individual knots in the chain of knots C (C1, C3, and C4) expanding towards the group of knots D, as one would expect in the scenario proposed by Nisini et al. (2001). The length of this flow would be ~ 0.84 or ~ 0.18 pc. If the 1.3 mm continuum source C is powering the flow C–D, then its t_{dyn} would be ~ 750 yr for a typical v_{jet} . It should be noted, however, that there

are also some knots in C expanding towards the chain of knots F, and there is an additional knot, labeled T, located between the knots chains F and C. This suggests a possible association of the strands of knots C, T, and F that could be part of the same flow (see Fig. 6a). The length of this possible flow would be ~ 1.8 or ~ 0.40 pc. In fact, Spitzer 4.5 μm observations seem to give support to this scenario, as the infrared emission connects F, T, and C (see Fig. 5). The two strands of knots C and F could be associated with the redshifted and blueshifted lobes, respectively, of the northern outflow orientated east-west mapped in CO ($J=2\rightarrow 1$) by Codella et al. (2001). Note that in this case, the redshifted lobe would be that of the outflow II, according to Nisini et al. (2001), while the blueshifted lobe would be that of the outflow III. Regarding the source powering this flow, it could be embedded in the dense gas detected in CS by Codella et al. (2001) and H¹³CO⁺ by Sugitani et al. (2002a). An emission peak, labeled as Core I, is visible in the Sugitani et al. maps. The high-density gas emission coincides with a high-extinction elongated region clearly visible in the J and H band maps (see Fig. 1). Therefore, a possible scenario could be the presence of two flows, one of them traced by the strands of knots F, T, and some knots of the C strand, and the other one by the group of knots D and some other individual knots of C. These two flows would collide towards the position of the chain of knots C, which would explain the strong H₂ emission towards this feature. Note that by extrapolating southwards the line that connects the chains of knots C, T, and F, one finds the group of knots labeled O, and by continuing farther south, the chain of knots B. Therefore, one could hypothesize that all these groups of knots could be related and be part of a long chain of H₂ emission knots. The total length of this long H₂ flow would be of ~ 3.1 or ~ 0.70 pc at the distance of IC 1396N.

From the morphology only it is difficult to confirm the possible flows observed in IC 1396N. To study the kinematics and physical conditions of the H₂ emission and determine whether different H₂ features that seem to be morphologically related are indeed part of the same long flow, additional long-slit NIR spectroscopy observations would be needed. In addition, if $v_{\text{jet}} \approx 150 \text{ km s}^{-1}$, then in about ~ 5 yr we should be able to cross-correlate the images and measure displacements of the knots of the order of the pixel size of NICS at the TNG. This way one could determine proper motions that would help to confirm or discard possible flows.

4. Summary and conclusions

We have carried out deep NIR observations at *J*, *H* and *K'* with NICS at the TNG telescope to study in detail the stellar population associated with the bright-rimmed cloud IC 1396N and reveal the presence of additional young sources inside the globule. The deep high-angular-resolution H₂ observations helped us to investigate the complex structure of this globule, and the morphology of the shocked gas that traces the interaction between the outflows in the region and the dense clumps surrounding the YSOs.

We have found 736 sources detected in all three bands within the area where the *JHK'* images overlap ($\sim 4.2 \times 4.2 \text{ arcmin}^2$). There are 128 sources detected only in *HK'*, 67 detected only in *K'*, and 79 detected only in *JH*. The completeness limits in the 2MASS standard are $K_s \sim 17.5$, $H \sim 18.5$ and $J \sim 19.5$. The sources with *HK'* or *K'* detections only are preferentially located towards the globule, whereas the sources with *JH* detections tend to be located outside the globule. Most of the stars in

the region either fall within the reddening band of the main sequence or exhibit only a small NIR excess as shown by the CCD. The source # 331, which coincides with source # 8 in Nisini et al. (2001) and HH77 IRS in Reipurth et al. (2003), is possibly a binary and the photometry has been derived for both A and B components. The sources of this system could be powering the major flow HH77 (Reipurth et al. (2003) and the H₂ flow G (Nisini et al. 2001). Although there are signatures of star formation in the globule, such as molecular outflows and jets, only the source # 331A exhibits a large NIR excess. This and source # 252 have been tentatively classified as Class I sources of intermediate-mass based on the CMD.

We have not found any color or age gradient in the south-north direction, indicative of the triggered star formation scenario suggested by Getman et al. (2007) from X-ray observations. We have not found either clear evidence of clustering of sources with NIR excess towards the southern edge of the globule. The evolutionary gradient found by Getman et al. (2007) may not correspond to an age gradient, since the intense UV radiation may have affected the circumstellar environments of the protostars close to the rim, suddenly stopping their growth and making them appear as less evolved Class II/III sources. Anyway, what is clear from NIR and millimeter observations is that not all the star formation in the globule can be explained in terms of triggering.

The H₂ emission is complex and knotty and shows a large number of molecular hydrogen features spread over the region, testifying a recent star-formation activity throughout the whole globule. The H₂ emission is resolved into several chains or groups of knots that sometimes show a jet-like morphology. This together with the fact that the knots are located in different parts of the globule suggest that the H₂ excitation is mostly due to shocks driven by outflows powered by YSOs. The shocked clodplet model scenario proposed by Beltrán et al. (2002) to explain the V-shaped morphology of the CO molecular outflow powered by BIMA 2 seems to be confirmed by the presence of H₂ emission (knots K1 and K2) at the position of the western clump B, which is causing the deflection of the outflow. The eastern deflecting clump R, visible in high-density tracers, is not visible in H₂, but this could be due to extinction. The H₂ emission of this BIMA 2 flow is visible farther east associated with the chain of knots A, probably when the emission reaches outside the core surrounding BIMA 2.

New possible flows have been discovered in the globule. One of them would be denoted by the group of knots E and those labeled P. Another flow would be traced by the strands of knots F, T, and some knots of the C strand. This flow would collide, towards the position of the chain of knots C, with the previously known flow C-D, denoted by the group of knots D and some individuals knots of C. The C-T-F flow could extend farther southwards up to reach the group of knots O or even the chain of knots B. Another possible flow has also been discovered towards the south of the globule that would be traced by the group of knots Q, HH593 and M, and could be powered by the YSO BIMA 3. This flow could extend up to reach some knots of the strand of knots B. In order to confirm these flows, additional long-slit NIR spectroscopy observations and proper motions determination would be needed.

Acknowledgements. This work is based on observations made with the Italian Telescopio Nazionale Galileo (TNG) operated on the island of La Palma by the Fundación Galileo Galilei of the INAF (Istituto Nazionale di Astrofisica) at the Spanish Observatorio del Roque de los Muchachos of the Instituto de Astrofisica de Canarias.

This work is based in part on observations made with the Spitzer Space Telescope, which is operated by the Jet Propulsion Laboratory, California Institute of Technology under a contract with NASA.

This publication makes use of data products from the Two Micron All Sky Survey, which is a joint project of the University of Massachusetts and the Infrared Processing and Analysis Center/California Institute of Technology, funded by the National Aeronautics and Space Administration and the National Science Foundation.

MTB, RL, JMG, and RE are supported by MEC grant AYA2005-08523-C03. JMG is also supported by AGAUR grant 2005SGR00489. FM acknowledges support from the Universitat de Barcelona during the data calibration process. This publication makes use of data products from the Two Micron All Sky Survey, which is a joint project of the University of Massachusetts and the Infrared Processing and Analysis Center/California Institute of Technology, funded by the National Aeronautics and Space Administration and the National Science Foundation.

References

- Allen, C. W. 1976, *Astrophysical Quantities* (3rd ed.), (London: Athlone press)
- Baffa, C., Comoretto, G., Gennari, S., et al. 2001, *A&A*, 378, 722
- Beltrán, M. T., Girart, J. M., Estalella, R., Ho, P. T. P., & Palau, A. 2002, *ApJ*, 573, 246
- Beltrán, M. T., Girart, J. M., Estalella, R., & Ho, P. T. P. 2004, *A&A*, 426, 941
- Caratti o Garatti, A., Giannini, T., Nisini, B., & Lorenzetti, D. 2006, *A&A*, 449, 1077
- Carpenter, J. M. 2001, *AJ*, 121, 285
- Codella, C., Bachiller, R., Nisini, B., Saraceno, P., Testi, L. 2001, *A&A*, 376, 271
- Correia, J. C. 2000, Ph.D. thesis, Univ. London
- Getman, K. V., Feigelson, E. D., Garmire, G., Broos, P., & Wang, J. 2007, *ApJ*, 654, 316
- Koornneef, J. 1983, *A&A*, 128, 84
- Lada, C. J., & Lada, E. A. 2003, *ARA&A*, 41, 57
- Matthews, T. J. 1979, *A&A*, 75, 345
- Neri, R., Fuente, A., Ceccarelli, C., Caselli, P. et al. 2007, *A&A*, 468, L33
- Nisini, B., Massi, F., Vitali, F., Giannini, T. et al. 2001, *A&A*, 376, 553
- Palla, F., & Stahler, S. W. 1991, *ApJ*, 375, 288
- Palla, F., & Stahler, S. W. 1999, *ApJ*, 525, 772
- Reipurth, B., Armond, T., Raga, A., & Bally, J. 2003, *ApJ*, 593, L47
- Reipurth, B., & Bally, J. 2001, *ARA&A*, 39, 403
- Rieke, G. H., & Lebofsky, M. J. 1985, *ApJ*, 288, 618
- Saraceno, P., Ceccarelli, C., Clegg, P., Correia, C. et al. 1996, *A&A*, 315, L293
- Smith, M. D., & Rosen, A. 2005, *MNRAS*, 357, 1370
- Sugitani, K., Fukui, Y., Mizuno, A., & Ohashi, N. 1989, *ApJ*, 342, L87
- Sugitani, K., Fukui, Y., & Ogura, K. 1991, *ApJS*, 77, 59
- Sugitani, K., Tamura, M., Nakaya, H., Nakajima, Y. et al. 2002a, *Proceedings of the IAU 8th Asian-Pacific Regional Meeting*, Vol. II, Ed. S. Ikeuchi, J. Hearnshaw, & T. Hanawa, (Tokyo: ASJ), 213
- Sugitani, K., Tamura, M., Nakajima, Y., Nagashima, C. et al. 2002b, *ApJL*, 565, L25
- Sugitani, K., Tamura, M., & Ogura, K. 1995, *ApJ*, 455, L39
- Vacca, W. D., Garmany, C. D., & Shull, J. M., 1996, *ApJ*, 460, 914
- Vanbeveren, D., De Loore, C., & Van Rensbergen, W. 1998, *A&AR*, 9, 63
- Walborn, N. R., & Panek, R. J., 1984, *ApJ*, 286, 718

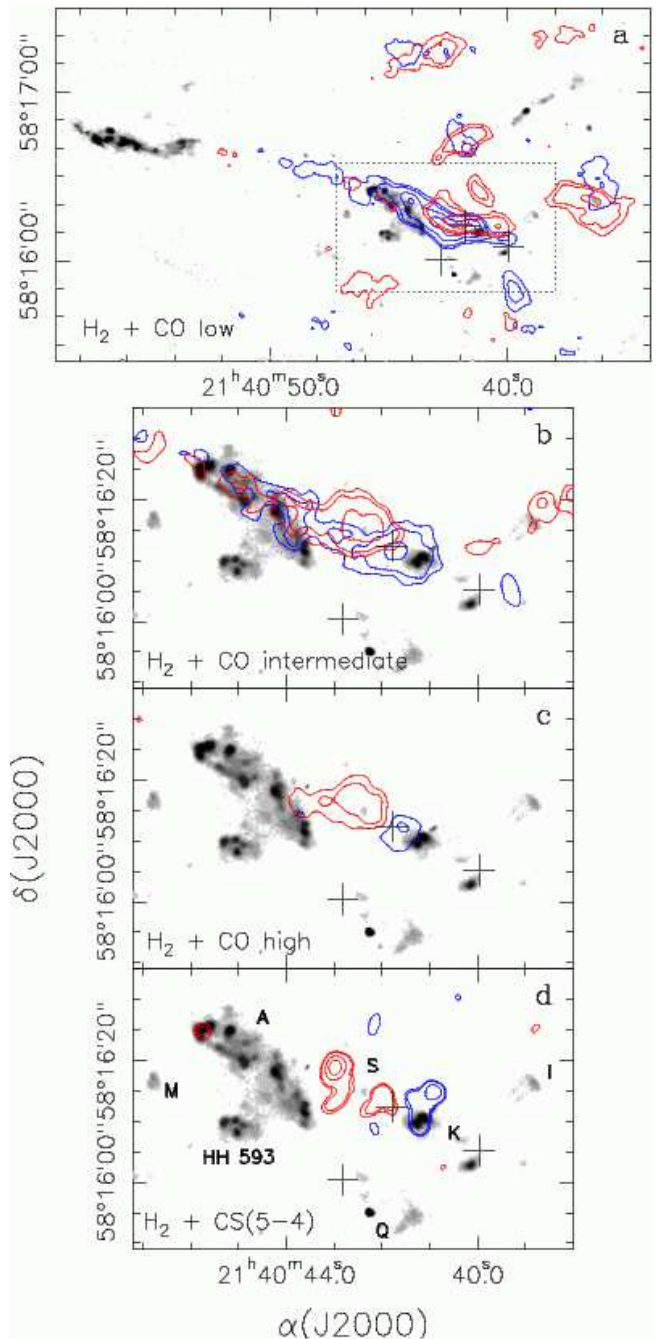


Fig. 7. (a): H_2 ($2.12 \mu\text{m}$) image (continuum-subtracted) in grey-scale and CO ($J=1 \rightarrow 0$) emission integrated in the $[\pm 3.5, \pm 9.5]$ km s^{-1} velocity interval in red and blue contours (Beltrán et al. 2002). (Lower panels): H_2 ($2.12 \mu\text{m}$) close-up image (continuum-subtracted), towards the position of BIMA 1, 2, and 3, in grey-scale and CO ($J=1 \rightarrow 0$) emission integrated in the $[\pm 9.5, \pm 15.5]$ km s^{-1} interval (b), and the $[\pm 15.5, \pm 21.5]$ km s^{-1} interval (c), and CS ($J=5 \rightarrow 4$) emission integrated in the $[\pm 5, \pm 12]$ km s^{-1} velocity interval (d), in red and blue contours (Beltrán et al. 2002). The black crosses show the positions of the 3.1 mm sources, BIMA 1, 2, and 3 from Beltrán et al. (2002).

Online Material

Table 1. JHK_s photometry and positions of found K_s sources detected in the three bands towards IC 1396N.

NIR source	α (J2000) ($^{\text{h}} \text{ m} \text{ s}$)	δ (J2000) ($^{\circ} \text{ ' } \text{ ''}$)	J	H (mag)	K_s
1	21 40 27.76	58 14 54.33	17.732 ± 0.014	16.970 ± 0.011	17.874 ± 0.126
2	21 40 43.25	58 14 54.51	17.788 ± 0.022	16.972 ± 0.016	17.681 ± 0.110
3	21 40 39.10	58 14 54.69	17.598 ± 0.012	16.938 ± 0.009	17.201 ± 0.076
5	21 40 42.12	58 14 54.82	17.419 ± 0.013	16.523 ± 0.009	16.439 ± 0.037
7	21 40 43.29	58 14 55.57	17.269 ± 0.011	16.590 ± 0.009	16.370 ± 0.028
8	21 40 32.01	58 14 56.29	16.370 ± 0.005	15.726 ± 0.004	15.601 ± 0.015
9	21 40 40.90	58 14 57.00	18.207 ± 0.035	17.506 ± 0.025	18.110 ± 0.103
10	21 40 28.82	58 14 57.15	18.116 ± 0.020	17.371 ± 0.014	17.657 ± 0.090
11	21 40 49.44	58 14 56.76	16.873 ± 0.006	16.284 ± 0.006	17.314 ± 0.046
12	21 40 21.60	58 14 57.90	15.124 ± 0.002	14.466 ± 0.002	14.488 ± 0.004
13	21 40 42.73	58 14 58.00	18.137 ± 0.025	17.437 ± 0.018	17.256 ± 0.044
14	21 40 41.35	58 14 58.08	18.206 ± 0.033	17.440 ± 0.027	17.488 ± 0.050
15	21 40 33.72	58 14 59.79	13.058 ± 0.025	12.092 ± 0.031	11.751 ± 0.023
16	21 40 33.37	58 15 00.37	17.097 ± 0.008	16.469 ± 0.009	16.464 ± 0.023
17	21 40 30.66	58 15 00.33	15.317 ± 0.002	14.849 ± 0.002	14.829 ± 0.004
18	21 40 48.78	58 15 00.25	17.248 ± 0.008	16.422 ± 0.005	16.554 ± 0.017
19	21 40 47.64	58 15 00.18	17.061 ± 0.007	16.388 ± 0.006	16.412 ± 0.016
21	21 40 26.17	58 15 01.24	19.009 ± 0.046	18.096 ± 0.036	15.837 ± 0.107
23	21 40 42.65	58 15 00.90	16.443 ± 0.004	15.944 ± 0.004	17.937 ± 0.013
22	21 40 45.19	58 15 01.00	19.009 ± 0.046	18.096 ± 0.036	18.152 ± 0.107
23	21 40 42.65	58 15 00.90	19.822 ± 0.106	18.423 ± 0.041	17.937 ± 0.085
24	21 40 36.38	58 15 01.45	18.283 ± 0.025	17.546 ± 0.021	17.944 ± 0.088
25	21 40 34.90	58 15 01.64	15.849 ± 0.003	15.362 ± 0.002	15.240 ± 0.007
26	21 40 30.00	58 15 03.00	17.486 ± 0.010	16.891 ± 0.009	17.064 ± 0.031
28	21 40 37.04	58 15 03.16	14.190 ± 0.001	13.232 ± 0.001	12.934 ± 0.001
29	21 40 38.80	58 15 03.49	16.956 ± 0.006	16.094 ± 0.004	15.958 ± 0.011
30	21 40 25.52	58 15 03.58	17.522 ± 0.011	17.036 ± 0.010	17.031 ± 0.038
31	21 40 44.84	58 15 03.53	14.581 ± 0.001	13.362 ± 0.001	12.935 ± 0.001
34	21 40 42.94	58 15 04.49	17.696 ± 0.012	16.598 ± 0.006	16.160 ± 0.015
35	21 40 46.24	58 15 05.76	17.284 ± 0.010	17.328 ± 0.015	17.204 ± 0.039
36	21 40 45.24	58 15 05.57	17.937 ± 0.019	17.090 ± 0.014	16.724 ± 0.025
37	21 40 29.78	58 15 06.30	17.496 ± 0.010	16.818 ± 0.008	17.055 ± 0.031
38	21 40 30.99	58 15 06.61	17.052 ± 0.011	16.621 ± 0.011	16.824 ± 0.024
39	21 40 39.70	58 15 06.88	16.593 ± 0.007	15.879 ± 0.005	15.522 ± 0.007
40	21 40 39.46	58 15 06.95	16.242 ± 0.004	15.546 ± 0.004	15.306 ± 0.006
41	21 40 46.15	58 15 07.12	15.746 ± 0.003	15.031 ± 0.002	14.750 ± 0.004
42	21 40 32.71	58 15 07.67	17.322 ± 0.008	16.362 ± 0.005	16.213 ± 0.010
43	21 40 51.37	58 15 08.45	18.858 ± 0.041	18.087 ± 0.029	17.869 ± 0.086
44	21 40 31.02	58 15 09.55	13.437 ± 0.029	12.972 ± 0.037	12.792 ± 0.035
45	21 40 23.90	58 15 10.00	16.546 ± 0.005	15.792 ± 0.004	15.648 ± 0.011
47	21 40 42.50	58 15 09.80	17.537 ± 0.011	16.217 ± 0.005	15.658 ± 0.009
48	21 40 34.14	58 15 10.88	16.920 ± 0.007	16.278 ± 0.005	16.224 ± 0.015
49	21 40 48.90	58 15 11.04	15.816 ± 0.003	15.126 ± 0.002	14.759 ± 0.003
51	21 40 41.16	58 15 11.42	12.968 ± 0.030	11.614 ± 0.035	10.676 ± 0.019
52	21 40 51.61	58 15 11.26	15.157 ± 0.002	14.460 ± 0.001	14.215 ± 0.003
53	21 40 46.56	58 15 11.47	18.037 ± 0.016	17.191 ± 0.011	16.881 ± 0.024
54	21 40 25.11	58 15 11.98	19.132 ± 0.047	18.137 ± 0.035	17.329 ± 0.055
55	21 40 45.50	58 15 11.69	14.714 ± 0.001	13.758 ± 0.001	13.295 ± 0.001
60	21 40 38.00	58 15 13.46	18.131 ± 0.017	17.151 ± 0.008	16.967 ± 0.026
62	21 40 44.33	58 15 13.43	16.315 ± 0.004	14.937 ± 0.002	14.103 ± 0.002
64	21 40 50.00	58 15 13.86	17.806 ± 0.014	17.120 ± 0.009	17.066 ± 0.023
65	21 40 34.66	58 15 14.30	17.457 ± 0.009	16.574 ± 0.005	16.371 ± 0.015
66	21 40 28.00	58 15 14.46	14.346 ± 0.001	13.361 ± 0.001	12.885 ± 0.001
67	21 40 39.05	58 15 14.45	17.912 ± 0.014	17.174 ± 0.009	16.950 ± 0.028
69	21 40 45.11	58 15 14.57	18.630 ± 0.030	17.221 ± 0.014	16.427 ± 0.021
70	21 40 52.42	58 15 14.74	18.612 ± 0.047	17.034 ± 0.011	16.813 ± 0.033
71	21 40 42.57	58 15 15.52	17.843 ± 0.013	17.125 ± 0.010	16.802 ± 0.028
72	21 40 41.28	58 15 15.75	17.108 ± 0.010	16.087 ± 0.007	15.606 ± 0.013
73	21 40 31.45	58 15 16.00	18.133 ± 0.023	17.381 ± 0.016	17.324 ± 0.035
75	21 40 49.77	58 15 15.77	18.283 ± 0.023	17.562 ± 0.016	17.275 ± 0.030
77	21 40 30.27	58 15 16.83	17.003 ± 0.007	16.357 ± 0.005	16.360 ± 0.014
79	21 40 20.10	58 15 18.75	15.597 ± 0.003	15.221 ± 0.003	15.111 ± 0.008
81	21 40 37.10	58 15 17.92	18.508 ± 0.033	17.693 ± 0.026	17.402 ± 0.056
83	21 40 27.93	58 15 18.40	16.700 ± 0.006	16.113 ± 0.005	15.912 ± 0.018
86	21 40 38.18	58 15 18.33	16.894 ± 0.005	16.206 ± 0.004	15.880 ± 0.011
90	21 40 41.16	58 15 19.14	18.102 ± 0.021	17.095 ± 0.013	16.432 ± 0.022
91	21 40 34.77	58 15 21.09	17.699 ± 0.012	16.683 ± 0.006	16.035 ± 0.012

Table 1. Continued.

NIR source	α (J2000) ($^{\text{h}} \text{ m } \text{s}$)	δ (J2000) ($^{\circ} \text{ } '$ '')	J	H (mag)	K_s
93	21 40 47.61	58 15 20.89	18.568 \pm 0.031	17.716 \pm 0.020	17.308 \pm 0.040
94	21 40 32.79	58 15 21.68	17.063 \pm 0.006	16.098 \pm 0.003	15.788 \pm 0.011
96	21 40 41.28	58 15 22.01	18.986 \pm 0.050	17.866 \pm 0.029	17.182 \pm 0.043
98	21 40 51.08	58 15 21.79	17.757 \pm 0.014	16.911 \pm 0.010	16.697 \pm 0.030
99	21 40 50.63	58 15 22.22	15.277 \pm 0.002	14.836 \pm 0.002	14.591 \pm 0.003
100	21 40 27.24	58 15 23.03	18.002 \pm 0.016	17.268 \pm 0.010	17.013 \pm 0.043
101	21 40 37.72	58 15 23.12	20.012 \pm 0.097	18.597 \pm 0.038	17.710 \pm 0.059
102	21 40 41.91	58 15 23.18	15.434 \pm 0.002	14.064 \pm 0.001	13.449 \pm 0.002
103	21 40 46.48	58 15 23.22	12.811 \pm 0.024	11.948 \pm 0.029	11.653 \pm 0.021
104	21 40 51.77	58 15 23.29	17.439 \pm 0.013	16.741 \pm 0.009	16.342 \pm 0.023
105	21 40 48.53	58 15 23.53	18.737 \pm 0.037	17.641 \pm 0.025	17.116 \pm 0.034
106	21 40 36.48	58 15 23.87	16.012 \pm 0.003	14.757 \pm 0.002	14.085 \pm 0.003
107	21 40 24.03	58 15 24.02	16.895 \pm 0.006	16.536 \pm 0.008	16.335 \pm 0.023
108	21 40 45.13	58 15 24.14	18.464 \pm 0.022	16.744 \pm 0.006	15.709 \pm 0.009
109	21 40 21.00	58 15 25.06	16.679 \pm 0.006	16.103 \pm 0.006	15.897 \pm 0.019
112	21 40 20.61	58 15 25.19	16.935 \pm 0.008	16.163 \pm 0.006	16.513 \pm 0.036
115	21 40 20.68	58 15 25.96	16.393 \pm 0.005	15.998 \pm 0.006	15.807 \pm 0.017
118	21 40 23.60	58 15 26.24	18.067 \pm 0.020	17.223 \pm 0.014	16.896 \pm 0.039
119	21 40 20.71	58 15 26.15	16.418 \pm 0.005	16.109 \pm 0.007	15.869 \pm 0.019
120	21 40 32.28	58 15 26.42	16.752 \pm 0.005	15.937 \pm 0.003	15.639 \pm 0.009
121	21 40 25.87	58 15 26.46	15.530 \pm 0.002	14.789 \pm 0.002	14.506 \pm 0.004
124	21 40 35.23	58 15 27.16	18.099 \pm 0.025	17.246 \pm 0.019	16.953 \pm 0.038
125	21 40 51.38	58 15 27.15	15.199 \pm 0.002	14.279 \pm 0.001	13.809 \pm 0.002
131	21 40 46.16	58 15 28.15	16.593 \pm 0.007	15.870 \pm 0.004	15.487 \pm 0.009
136	21 40 35.13	58 15 31.12	18.209 \pm 0.018	16.847 \pm 0.008	16.158 \pm 0.015
140	21 40 39.61	58 15 32.31	18.494 \pm 0.020	17.137 \pm 0.009	16.363 \pm 0.015
141	21 40 51.10	58 15 32.38	18.567 \pm 0.034	17.556 \pm 0.018	17.112 \pm 0.038
142	21 40 25.32	58 15 33.20	17.709 \pm 0.011	17.142 \pm 0.010	16.816 \pm 0.031
145	21 40 46.88	58 15 33.54	15.288 \pm 0.002	13.573 \pm 0.001	12.675 \pm 0.001
146	21 40 47.51	58 15 33.75	17.496 \pm 0.012	15.583 \pm 0.005	14.515 \pm 0.004
148	21 40 51.91	58 15 33.96	16.647 \pm 0.010	15.955 \pm 0.008	15.553 \pm 0.015
149	21 40 22.82	58 15 35.66	18.100 \pm 0.020	17.240 \pm 0.017	16.745 \pm 0.031
152	21 40 49.32	58 15 34.93	20.097 \pm 0.100	18.232 \pm 0.027	17.115 \pm 0.027
154	21 40 51.83	58 15 35.14	16.617 \pm 0.012	15.978 \pm 0.014	15.539 \pm 0.017
155	21 40 40.02	58 15 35.47	19.590 \pm 0.060	17.462 \pm 0.013	16.403 \pm 0.014
157	21 40 51.60	58 15 35.79	16.499 \pm 0.006	15.803 \pm 0.004	15.284 \pm 0.009
158	21 40 39.56	58 15 36.24	20.200 \pm 0.094	17.809 \pm 0.019	16.577 \pm 0.017
159	21 40 32.70	58 15 36.76	17.263 \pm 0.007	16.601 \pm 0.005	16.382 \pm 0.016
160	21 40 19.84	58 15 36.89	17.426 \pm 0.013	16.863 \pm 0.015	16.521 \pm 0.027
161	21 40 51.90	58 15 36.79	15.502 \pm 0.003	14.571 \pm 0.002	14.212 \pm 0.004
164	21 40 48.02	58 15 37.78	13.823 \pm 0.001	12.991 \pm 0.001	12.571 \pm 0.001
165	21 40 40.88	58 15 38.94	19.985 \pm 0.079	18.495 \pm 0.033	17.725 \pm 0.053
166	21 40 37.56	58 15 39.53	18.071 \pm 0.017	16.983 \pm 0.010	16.237 \pm 0.017
167	21 40 25.88	58 15 39.94	18.720 \pm 0.029	18.040 \pm 0.024	17.546 \pm 0.061
170	21 40 38.83	58 15 39.73	20.454 \pm 0.135	18.200 \pm 0.026	16.987 \pm 0.025
173	21 40 45.86	58 15 40.63	18.705 \pm 0.028	17.088 \pm 0.008	16.013 \pm 0.010
174	21 40 47.19	58 15 41.51	18.429 \pm 0.023	16.520 \pm 0.006	15.324 \pm 0.005
177	21 40 47.46	58 15 43.12	18.736 \pm 0.036	17.967 \pm 0.019	17.599 \pm 0.049
178	21 40 21.15	58 15 43.75	16.506 \pm 0.005	15.644 \pm 0.004	15.226 \pm 0.008
179	21 40 50.12	58 15 43.49	19.983 \pm 0.102	17.632 \pm 0.017	16.387 \pm 0.015
183	21 40 33.09	58 15 44.99	19.154 \pm 0.051	17.661 \pm 0.021	16.963 \pm 0.031
184	21 40 51.89	58 15 44.56	15.800 \pm 0.004	14.266 \pm 0.001	13.519 \pm 0.002
185	21 40 42.83	58 15 45.46	16.291 \pm 0.004	15.375 \pm 0.002	14.767 \pm 0.003
186	21 40 25.10	58 15 46.54	17.512 \pm 0.012	16.912 \pm 0.011	16.463 \pm 0.028
187	21 40 37.17	58 15 46.76	17.073 \pm 0.009	15.457 \pm 0.003	14.503 \pm 0.003
188	21 40 28.72	58 15 46.68	18.714 \pm 0.028	17.798 \pm 0.017	17.606 \pm 0.060
190	21 40 30.95	58 15 47.73	17.610 \pm 0.012	16.601 \pm 0.008	16.268 \pm 0.013
191	21 40 25.41	58 15 47.47	15.269 \pm 0.002	14.607 \pm 0.002	14.217 \pm 0.003
193	21 40 32.87	58 15 48.31	17.422 \pm 0.011	16.612 \pm 0.008	16.087 \pm 0.014
201	21 40 28.48	58 15 50.94	18.420 \pm 0.022	17.751 \pm 0.017	17.468 \pm 0.053
205	21 40 44.58	58 15 51.79	15.974 \pm 0.003	15.235 \pm 0.002	14.706 \pm 0.003
208	21 40 31.42	58 15 52.44	18.629 \pm 0.025	17.650 \pm 0.021	17.230 \pm 0.042
210	21 40 42.09	58 15 52.75	16.611 \pm 0.005	15.505 \pm 0.004	14.791 \pm 0.004
211	21 40 28.38	58 15 53.14	18.430 \pm 0.023	17.751 \pm 0.020	17.431 \pm 0.057
215	21 40 27.99	58 15 54.32	18.364 \pm 0.025	17.562 \pm 0.017	17.146 \pm 0.043
217	21 40 41.04	58 15 54.49	17.113 \pm 0.008	16.402 \pm 0.009	16.013 \pm 0.023
220	21 40 28.43	58 15 56.90	17.646 \pm 0.010	16.857 \pm 0.007	16.572 \pm 0.021

Table 1. Continued.

NIR source	α (J2000) ($^{\text{h}} \text{ m } \text{s}$)	δ (J2000) ($^{\circ} \text{ } '$ '')	J	H (mag)	K_s
225	21 40 27.38	58 16 00.23	17.886 \pm 0.013	17.200 \pm 0.009	16.875 \pm 0.030
227	21 40 48.60	58 16 01.06	15.575 \pm 0.002	13.305 \pm 0.001	11.843 \pm 0.001
229	21 40 31.59	58 16 02.11	18.084 \pm 0.017	16.858 \pm 0.007	16.185 \pm 0.012
230	21 40 28.11	58 16 02.48	18.662 \pm 0.023	17.865 \pm 0.019	17.544 \pm 0.054
232	21 40 45.51	58 16 02.81	15.712 \pm 0.003	13.795 \pm 0.001	12.829 \pm 0.001
233	21 40 32.48	58 16 03.79	18.908 \pm 0.036	17.045 \pm 0.008	16.059 \pm 0.011
236	21 40 44.83	58 16 05.19	16.815 \pm 0.012	14.331 \pm 0.002	12.976 \pm 0.001
238	21 40 46.06	58 16 06.11	18.141 \pm 0.020	16.612 \pm 0.008	15.719 \pm 0.007
239	21 40 20.10	58 16 08.30	16.482 \pm 0.005	15.883 \pm 0.005	15.575 \pm 0.010
240	21 40 27.98	58 16 08.44	16.947 \pm 0.006	16.251 \pm 0.004	15.909 \pm 0.011
242	21 40 29.27	58 16 08.98	17.714 \pm 0.010	17.163 \pm 0.008	16.925 \pm 0.022
243	21 40 23.66	58 16 09.14	17.928 \pm 0.014	17.037 \pm 0.011	16.577 \pm 0.024
244	21 40 48.66	58 16 09.06	20.075 \pm 0.102	18.755 \pm 0.046	17.581 \pm 0.044
245	21 40 44.67	58 16 09.37	18.219 \pm 0.046	17.165 \pm 0.034	16.437 \pm 0.048
247	21 40 31.19	58 16 10.29	17.236 \pm 0.009	16.204 \pm 0.004	15.721 \pm 0.008
248	21 40 24.99	58 16 10.74	14.371 \pm 0.001	13.739 \pm 0.001	13.341 \pm 0.002
249	21 40 24.47	58 16 10.76	17.993 \pm 0.021	17.076 \pm 0.016	16.587 \pm 0.028
250	21 40 22.27	58 16 11.92	16.704 \pm 0.005	16.060 \pm 0.005	15.739 \pm 0.010
253	21 40 21.46	58 16 12.87	18.079 \pm 0.017	17.136 \pm 0.012	16.794 \pm 0.028
257	21 40 25.64	58 16 13.80	17.964 \pm 0.019	16.906 \pm 0.009	16.406 \pm 0.020
258	21 40 47.48	58 16 14.08	20.215 \pm 0.106	18.311 \pm 0.039	17.249 \pm 0.036
259	21 40 30.67	58 16 14.52	18.133 \pm 0.019	17.129 \pm 0.009	16.680 \pm 0.015
260	21 40 45.80	58 16 14.84	19.966 \pm 0.110	18.586 \pm 0.056	17.925 \pm 0.070
261	21 40 20.83	58 16 15.55	14.149 \pm 0.034	13.510 \pm 0.041	13.306 \pm 0.039
263	21 40 27.04	58 16 16.08	16.801 \pm 0.005	15.943 \pm 0.003	15.532 \pm 0.008
265	21 40 24.09	58 16 16.92	17.614 \pm 0.011	16.465 \pm 0.007	15.971 \pm 0.015
266	21 40 21.47	58 16 17.75	17.941 \pm 0.016	16.966 \pm 0.010	16.568 \pm 0.024
267	21 40 24.89	58 16 18.03	17.213 \pm 0.007	16.458 \pm 0.006	16.001 \pm 0.014
268	21 40 29.07	58 16 18.01	17.185 \pm 0.007	16.482 \pm 0.004	16.148 \pm 0.013
269	21 40 45.51	58 16 18.03	19.682 \pm 0.076	18.394 \pm 0.041	17.768 \pm 0.061
272	21 40 28.28	58 16 19.33	19.128 \pm 0.036	18.231 \pm 0.022	17.834 \pm 0.059
273	21 40 48.28	58 16 19.09	18.171 \pm 0.020	17.158 \pm 0.013	16.400 \pm 0.017
275	21 40 24.32	58 16 20.03	17.685 \pm 0.014	16.845 \pm 0.009	16.499 \pm 0.023
277	21 40 43.56	58 16 20.81	18.377 \pm 0.021	17.609 \pm 0.019	17.027 \pm 0.049
280	21 40 27.97	58 16 22.47	18.188 \pm 0.017	17.339 \pm 0.010	16.935 \pm 0.026
281	21 40 29.29	58 16 22.65	16.628 \pm 0.006	15.888 \pm 0.004	15.510 \pm 0.009
283	21 40 48.86	58 16 23.01	16.058 \pm 0.003	15.163 \pm 0.002	14.598 \pm 0.003
285	21 40 29.17	58 16 23.63	17.957 \pm 0.018	17.360 \pm 0.016	16.931 \pm 0.035
287	21 40 22.09	58 16 24.40	16.178 \pm 0.003	15.632 \pm 0.003	15.340 \pm 0.008
288	21 40 51.98	58 16 23.80	19.205 \pm 0.059	17.465 \pm 0.014	16.394 \pm 0.014
290	21 40 29.06	58 16 24.76	17.869 \pm 0.017	17.103 \pm 0.011	16.729 \pm 0.027
291	21 40 51.08	58 16 24.50	17.800 \pm 0.013	16.700 \pm 0.007	16.089 \pm 0.010
293	21 40 31.94	58 16 26.58	19.885 \pm 0.095	17.787 \pm 0.020	16.823 \pm 0.021
294	21 40 27.16	58 16 26.83	17.993 \pm 0.015	17.208 \pm 0.009	16.810 \pm 0.021
296	21 40 48.63	58 16 26.37	17.800 \pm 0.015	16.525 \pm 0.008	15.849 \pm 0.010
297	21 40 45.71	58 16 27.41	18.982 \pm 0.043	16.709 \pm 0.009	15.522 \pm 0.009
298	21 40 21.11	58 16 28.39	17.997 \pm 0.014	17.210 \pm 0.013	16.914 \pm 0.033
301	21 40 22.55	58 16 28.99	16.353 \pm 0.004	15.666 \pm 0.004	15.386 \pm 0.008
305	21 40 51.82	58 16 29.39	15.636 \pm 0.003	14.339 \pm 0.001	13.709 \pm 0.002
307	21 40 22.30	58 16 32.86	14.877 \pm 0.001	14.259 \pm 0.001	13.997 \pm 0.003
310	21 40 22.11	58 16 33.67	17.167 \pm 0.009	16.561 \pm 0.009	16.170 \pm 0.018
311	21 40 27.85	58 16 33.93	18.426 \pm 0.027	17.711 \pm 0.018	17.527 \pm 0.055
314	21 40 19.61	58 16 34.53	18.525 \pm 0.064	17.734 \pm 0.033	17.369 \pm 0.051
317	21 40 30.04	58 16 34.89	18.287 \pm 0.023	17.153 \pm 0.011	16.695 \pm 0.020
322	21 40 26.23	58 16 37.26	17.673 \pm 0.014	17.082 \pm 0.011	16.757 \pm 0.025
326	21 40 48.54	58 16 37.31	16.217 \pm 0.004	15.035 \pm 0.002	14.333 \pm 0.002
328	21 40 51.78	58 16 37.56	19.947 \pm 0.150	18.660 \pm 0.060	17.876 \pm 0.096
329	21 40 47.36	58 16 37.56	18.999 \pm 0.036	16.134 \pm 0.004	14.661 \pm 0.003
330	21 40 27.97	58 16 38.13	15.996 \pm 0.005	15.284 \pm 0.004	14.982 \pm 0.008
331A ^a	21 40 41.44	58 16 38.10	19.178 \pm 0.055	16.032 \pm 0.041	13.109 \pm 0.046
332	21 40 32.66	58 16 38.32	19.500 \pm 0.074	17.735 \pm 0.018	16.833 \pm 0.025
333	21 40 26.14	58 16 38.79	17.297 \pm 0.010	16.576 \pm 0.006	16.255 \pm 0.015
334	21 40 48.80	58 16 38.51	19.290 \pm 0.060	18.503 \pm 0.050	17.870 \pm 0.060
335	21 40 51.45	58 16 38.69	17.301 \pm 0.014	17.082 \pm 0.017	16.538 \pm 0.029
336	21 40 28.06	58 16 38.92	16.788 \pm 0.013	16.576 \pm 0.018	16.080 \pm 0.028
337	21 40 51.24	58 16 39.15	14.168 \pm 0.001	13.639 \pm 0.001	13.408 \pm 0.002
338	21 40 26.83	58 16 39.73	18.828 \pm 0.037	17.856 \pm 0.019	17.497 \pm 0.054

Table 1. Continued.

NIR source	α (J2000) ($^{\text{h}} \text{ m } \text{s}$)	δ (J2000) ($^{\circ} \text{ } '$ '')	J	H (mag)	K_s
339	21 40 29.13	58 16 39.99	18.151 ± 0.031	17.108 ± 0.018	16.651 ± 0.034
340	21 40 22.32	58 16 40.09	18.418 ± 0.024	17.734 ± 0.021	17.420 ± 0.054
342	21 40 30.15	58 16 40.43	18.547 ± 0.030	17.500 ± 0.014	16.922 ± 0.028
343	21 40 22.94	58 16 41.34	18.080 ± 0.017	17.296 ± 0.015	16.988 ± 0.031
345	21 40 27.70	58 16 41.51	17.440 ± 0.016	16.625 ± 0.011	16.219 ± 0.027
347	21 40 45.25	58 16 41.59	17.376 ± 0.011	16.296 ± 0.006	15.531 ± 0.007
349	21 40 28.37	58 16 42.51	11.593 ± 0.023	10.784 ± 0.030	10.434 ± 0.021
352	21 40 26.76	58 16 43.77	17.914 ± 0.015	17.219 ± 0.011	16.856 ± 0.031
354	21 40 50.88	58 16 43.29	19.725 ± 0.087	18.673 ± 0.051	18.198 ± 0.087
359	21 40 45.42	58 16 45.80	20.384 ± 0.152	17.484 ± 0.015	15.961 ± 0.009
360	21 40 19.81	58 16 46.83	17.989 ± 0.026	17.330 ± 0.022	16.921 ± 0.030
363	21 40 23.14	58 16 48.03	17.014 ± 0.007	16.213 ± 0.005	15.905 ± 0.012
365	21 40 30.14	58 16 49.10	16.837 ± 0.007	16.106 ± 0.005	15.729 ± 0.009
366	21 40 33.51	58 16 49.78	18.028 ± 0.019	16.662 ± 0.007	15.939 ± 0.010
368	21 40 35.53	58 16 50.13	19.900 ± 0.105	18.271 ± 0.037	17.520 ± 0.043
371	21 40 19.96	58 16 51.10	18.662 ± 0.037	17.779 ± 0.028	17.276 ± 0.039
374	21 40 25.09	58 16 52.56	16.505 ± 0.004	15.915 ± 0.004	15.564 ± 0.010
375	21 40 32.52	58 16 52.73	18.763 ± 0.048	17.361 ± 0.024	16.410 ± 0.028
377	21 40 40.99	58 16 52.66	17.871 ± 0.016	15.345 ± 0.003	14.070 ± 0.002
378	21 40 28.63	58 16 53.05	19.355 ± 0.063	18.517 ± 0.040	17.964 ± 0.111
380	21 40 36.07	58 16 52.99	18.080 ± 0.020	16.581 ± 0.007	15.906 ± 0.009
381	21 40 31.51	58 16 53.10	18.804 ± 0.042	17.663 ± 0.020	17.092 ± 0.035
382	21 40 48.32	58 16 53.01	19.490 ± 0.058	17.381 ± 0.016	16.125 ± 0.013
383	21 40 33.45	58 16 53.65	20.284 ± 0.143	18.323 ± 0.030	17.363 ± 0.036
385	21 40 32.24	58 16 53.79	14.132 ± 0.028	12.437 ± 0.035	11.708 ± 0.026
386	21 40 35.29	58 16 54.21	18.315 ± 0.023	16.666 ± 0.007	15.842 ± 0.010
387	21 40 38.57	58 16 54.99	19.455 ± 0.074	17.625 ± 0.020	16.515 ± 0.020
389	21 40 24.84	58 16 55.95	19.188 ± 0.045	18.117 ± 0.028	17.760 ± 0.073
390	21 40 34.06	58 16 57.43	19.439 ± 0.077	17.873 ± 0.021	17.225 ± 0.035
392	21 40 34.29	58 16 57.81	19.767 ± 0.101	17.937 ± 0.022	17.202 ± 0.031
393	21 40 21.52	58 16 58.16	17.753 ± 0.012	16.752 ± 0.009	16.395 ± 0.019
394	21 40 23.66	58 16 58.26	18.239 ± 0.019	17.635 ± 0.022	17.301 ± 0.052
395	21 40 50.26	58 16 58.57	19.666 ± 0.067	18.431 ± 0.036	17.759 ± 0.059
399	21 40 26.30	58 17 00.13	16.662 ± 0.005	15.993 ± 0.003	15.658 ± 0.009
400	21 40 33.77	58 17 00.12	19.354 ± 0.062	17.719 ± 0.018	16.827 ± 0.025
401	21 40 22.79	58 17 00.71	16.477 ± 0.004	15.811 ± 0.004	15.522 ± 0.009
404	21 40 48.88	58 17 00.22	18.844 ± 0.034	17.368 ± 0.012	16.598 ± 0.018
405	21 40 35.31	58 17 00.97	18.111 ± 0.020	16.455 ± 0.007	15.585 ± 0.008
407	21 40 49.51	58 17 00.60	19.398 ± 0.056	18.180 ± 0.028	17.453 ± 0.039
408	21 40 20.28	58 17 01.76	19.653 ± 0.077	17.982 ± 0.030	16.968 ± 0.032
410	21 40 47.41	58 17 01.38	19.071 ± 0.048	16.679 ± 0.008	15.432 ± 0.007
411	21 40 31.22	58 17 01.67	19.412 ± 0.072	18.167 ± 0.025	17.557 ± 0.042
412	21 40 47.78	58 17 01.63	15.633 ± 0.002	14.862 ± 0.002	14.494 ± 0.004
415	21 40 25.87	58 17 02.79	19.209 ± 0.047	18.224 ± 0.027	17.714 ± 0.070
417	21 40 28.73	58 17 02.86	18.219 ± 0.018	17.324 ± 0.011	16.785 ± 0.038
421	21 40 49.05	58 17 04.22	19.235 ± 0.055	17.659 ± 0.020	16.889 ± 0.025
422	21 40 36.54	58 17 04.86	17.632 ± 0.015	17.652 ± 0.024	16.871 ± 0.034
424	21 40 24.82	58 17 05.49	18.494 ± 0.026	17.468 ± 0.018	17.041 ± 0.041
425	21 40 44.65	58 17 05.13	17.229 ± 0.007	15.458 ± 0.003	14.208 ± 0.002
427	21 40 34.41	58 17 05.82	18.278 ± 0.024	16.933 ± 0.009	16.222 ± 0.014
428	21 40 36.62	58 17 06.21	16.253 ± 0.004	14.735 ± 0.002	13.982 ± 0.002
433	21 40 25.78	58 17 07.89	16.638 ± 0.004	16.223 ± 0.004	15.899 ± 0.012
434	21 40 52.46	58 17 07.36	17.213 ± 0.022	16.647 ± 0.006	16.110 ± 0.018
435	21 40 24.50	58 17 08.14	16.343 ± 0.004	15.799 ± 0.005	15.444 ± 0.010
439	21 40 25.10	58 17 08.97	18.150 ± 0.016	17.474 ± 0.016	17.085 ± 0.041
440	21 40 24.67	58 17 09.38	16.653 ± 0.005	16.251 ± 0.006	15.975 ± 0.016
442	21 40 49.07	58 17 09.53	14.121 ± 0.001	12.795 ± 0.001	12.016 ± 0.001
447	21 40 30.75	58 17 11.11	17.514 ± 0.011	16.518 ± 0.005	16.050 ± 0.010
448	21 40 25.76	58 17 11.79	18.831 ± 0.033	18.016 ± 0.024	17.740 ± 0.079
449	21 40 40.53	58 17 11.75	19.114 ± 0.053	17.396 ± 0.015	16.504 ± 0.019
452	21 40 25.51	58 17 12.75	17.537 ± 0.009	17.069 ± 0.009	16.708 ± 0.029
454	21 40 49.30	58 17 12.17	18.444 ± 0.027	17.384 ± 0.016	16.728 ± 0.023
456	21 40 28.12	58 17 13.75	18.450 ± 0.022	17.594 ± 0.015	17.184 ± 0.049
457	21 40 23.78	58 17 14.62	17.090 ± 0.006	16.441 ± 0.006	16.080 ± 0.017
462	21 40 49.04	58 17 17.23	17.431 ± 0.010	16.109 ± 0.005	15.371 ± 0.007
464	21 40 21.82	58 17 18.60	18.963 ± 0.038	18.154 ± 0.028	17.926 ± 0.077
467	21 40 33.49	58 17 18.66	19.755 ± 0.101	18.255 ± 0.034	17.493 ± 0.051

Table 1. Continued.

NIR source	α (J2000) ($^{\text{h}} \text{ m } \text{s}$)	δ (J2000) ($^{\circ} \text{ } '$ '')	J	H (mag)	K_s
468	21 40 25.08	58 17 18.87	18.042 \pm 0.015	17.823 \pm 0.021	17.366 \pm 0.051
469	21 40 23.21	58 17 19.04	18.418 \pm 0.021	17.791 \pm 0.020	17.517 \pm 0.057
472	21 40 25.14	58 17 20.06	17.940 \pm 0.013	17.326 \pm 0.011	17.101 \pm 0.043
473	21 40 49.06	58 17 19.77	15.582 \pm 0.002	13.782 \pm 0.001	12.938 \pm 0.001
475	21 40 27.11	58 17 20.82	17.823 \pm 0.012	17.202 \pm 0.009	16.908 \pm 0.035
477	21 40 26.86	58 17 21.33	18.890 \pm 0.033	18.203 \pm 0.027	17.810 \pm 0.072
481	21 40 24.13	58 17 22.17	17.208 \pm 0.008	16.701 \pm 0.008	16.416 \pm 0.024
483	21 40 34.77	58 17 23.39	19.834 \pm 0.106	18.343 \pm 0.036	17.722 \pm 0.057
484	21 40 33.65	58 17 23.32	18.134 \pm 0.026	17.091 \pm 0.012	16.602 \pm 0.021
486	21 40 51.82	58 17 23.10	19.318 \pm 0.076	18.271 \pm 0.029	17.749 \pm 0.083
487	21 40 32.74	58 17 23.73	12.191 \pm 0.023	11.551 \pm 0.031	11.359 \pm 0.026
488	21 40 47.63	58 17 23.45	19.864 \pm 0.083	18.346 \pm 0.025	17.538 \pm 0.038
489	21 40 35.20	58 17 24.98	16.929 \pm 0.007	15.766 \pm 0.003	15.154 \pm 0.005
490	21 40 26.71	58 17 25.19	17.869 \pm 0.013	17.256 \pm 0.011	16.957 \pm 0.036
491	21 40 29.46	58 17 25.63	17.786 \pm 0.012	17.191 \pm 0.011	16.834 \pm 0.030
493	21 40 32.50	58 17 25.73	17.333 \pm 0.018	16.519 \pm 0.012	15.945 \pm 0.016
495	21 40 31.10	58 17 27.06	19.367 \pm 0.053	18.219 \pm 0.029	17.644 \pm 0.043
496	21 40 49.77	58 17 26.86	18.398 \pm 0.021	16.628 \pm 0.007	15.760 \pm 0.009
497	21 40 23.36	58 17 27.88	19.046 \pm 0.040	17.913 \pm 0.027	17.226 \pm 0.043
499	21 40 28.03	58 17 28.34	15.721 \pm 0.003	14.866 \pm 0.002	14.416 \pm 0.004
501	21 40 34.04	58 17 29.74	17.565 \pm 0.013	16.705 \pm 0.007	16.198 \pm 0.014
503	21 40 24.70	58 17 30.73	12.617 \pm 0.026	11.822 \pm 0.028	11.545 \pm 0.021
506	21 40 34.16	58 17 32.45	18.691 \pm 0.036	17.498 \pm 0.015	16.969 \pm 0.027
508	21 40 31.88	58 17 32.93	17.824 \pm 0.013	16.988 \pm 0.010	16.559 \pm 0.018
509	21 40 32.67	58 17 33.14	19.129 \pm 0.052	18.068 \pm 0.027	17.495 \pm 0.040
510	21 40 20.51	58 17 33.64	18.406 \pm 0.022	17.405 \pm 0.017	17.053 \pm 0.035
511	21 40 26.09	58 17 33.66	17.913 \pm 0.014	17.325 \pm 0.011	17.060 \pm 0.035
512	21 40 21.50	58 17 33.99	17.837 \pm 0.019	16.995 \pm 0.020	16.595 \pm 0.035
513	21 40 34.67	58 17 34.06	19.044 \pm 0.048	18.012 \pm 0.022	17.387 \pm 0.040
514	21 40 31.03	58 17 34.01	15.595 \pm 0.002	14.606 \pm 0.002	14.172 \pm 0.002
517	21 40 28.75	58 17 34.25	19.504 \pm 0.061	18.305 \pm 0.032	17.813 \pm 0.086
519	21 40 19.80	58 17 34.67	15.605 \pm 0.003	15.094 \pm 0.003	14.709 \pm 0.004
520	21 40 47.62	58 17 35.51	16.906 \pm 0.009	15.902 \pm 0.008	15.303 \pm 0.010
524	21 40 48.35	58 17 37.21	19.584 \pm 0.082	18.237 \pm 0.045	17.566 \pm 0.072
525	21 40 27.34	58 17 37.96	18.077 \pm 0.017	17.361 \pm 0.011	16.949 \pm 0.031
527	21 40 49.68	58 17 37.50	16.672 \pm 0.005	14.957 \pm 0.002	14.120 \pm 0.002
528	21 40 21.38	58 17 38.24	17.016 \pm 0.009	16.361 \pm 0.007	16.064 \pm 0.021
529	21 40 39.10	58 17 38.14	20.102 \pm 0.133	17.386 \pm 0.017	16.021 \pm 0.011
531	21 40 47.49	58 17 39.40	11.534 \pm 0.026	9.985 \pm 0.029	9.373 \pm 0.023
533	21 40 51.65	58 17 40.31	17.901 \pm 0.018	16.538 \pm 0.006	15.823 \pm 0.014
538	21 40 31.08	58 17 44.02	17.556 \pm 0.009	16.738 \pm 0.006	16.373 \pm 0.014
540	21 40 23.79	58 17 46.20	17.898 \pm 0.013	17.037 \pm 0.011	16.597 \pm 0.021
542	21 40 52.27	58 17 46.21	15.596 \pm 0.004	14.557 \pm 0.002	13.960 \pm 0.002
543	21 40 25.12	58 17 46.93	18.592 \pm 0.035	17.922 \pm 0.025	17.492 \pm 0.052
544	21 40 32.55	58 17 47.66	18.383 \pm 0.021	17.534 \pm 0.015	17.117 \pm 0.033
545	21 40 36.92	58 17 48.00	19.793 \pm 0.081	17.557 \pm 0.014	16.429 \pm 0.014
548	21 40 49.21	58 17 48.11	17.768 \pm 0.014	16.826 \pm 0.008	16.247 \pm 0.013
549	21 40 49.42	58 17 48.14	20.011 \pm 0.110	18.335 \pm 0.032	17.723 \pm 0.047
551	21 40 20.54	58 17 49.43	16.617 \pm 0.006	16.154 \pm 0.005	15.819 \pm 0.011
552	21 40 36.45	58 17 49.62	20.321 \pm 0.140	18.797 \pm 0.046	17.864 \pm 0.052
554	21 40 29.82	58 17 51.40	17.546 \pm 0.010	16.875 \pm 0.006	16.587 \pm 0.018
556	21 40 30.53	58 17 52.21	16.643 \pm 0.005	16.846 \pm 0.010	16.521 \pm 0.020
558	21 40 46.48	58 17 52.26	20.511 \pm 0.151	18.658 \pm 0.039	17.851 \pm 0.063
559	21 40 30.61	58 17 53.10	15.654 \pm 0.002	15.106 \pm 0.002	14.807 \pm 0.004
560	21 40 30.34	58 17 53.06	16.866 \pm 0.006	16.130 \pm 0.004	15.795 \pm 0.010
562	21 40 49.35	58 17 52.97	18.972 \pm 0.038	17.848 \pm 0.018	17.308 \pm 0.035
563	21 40 20.71	58 17 53.63	18.556 \pm 0.027	17.585 \pm 0.022	17.195 \pm 0.040
564	21 40 41.10	58 17 54.43	14.106 \pm 0.001	13.423 \pm 0.001	13.135 \pm 0.001
565	21 40 33.60	58 17 55.00	18.364 \pm 0.022	17.237 \pm 0.012	16.596 \pm 0.025
567	21 40 32.54	58 17 55.32	18.796 \pm 0.029	17.856 \pm 0.017	17.386 \pm 0.038
568	21 40 31.59	58 17 55.31	13.865 \pm 0.001	12.766 \pm 0.001	12.231 \pm 0.001
569	21 40 30.03	58 17 55.99	18.316 \pm 0.022	17.427 \pm 0.013	17.049 \pm 0.026
570	21 40 49.79	58 17 55.72	19.972 \pm 0.096	18.243 \pm 0.027	17.422 \pm 0.036
573	21 40 31.75	58 17 57.92	18.673 \pm 0.031	17.594 \pm 0.018	17.232 \pm 0.043
574	21 40 28.29	58 18 00.32	17.066 \pm 0.007	16.362 \pm 0.005	15.952 \pm 0.010
577	21 40 48.63	58 18 00.70	15.861 \pm 0.003	15.162 \pm 0.002	14.691 \pm 0.003
580	21 40 20.28	58 18 02.16	18.859 \pm 0.043	17.726 \pm 0.026	17.425 \pm 0.047

Table 1. Continued.

NIR source	α (J2000) ($^{\text{h}} \text{ m } \text{s}$)	δ (J2000) ($^{\circ} \text{ } '$ '')	J	H (mag)	K_s
582	21 40 21.84	58 18 02.63	17.892 ± 0.013	17.176 ± 0.013	16.870 ± 0.031
584	21 40 19.93	58 18 04.64	19.291 ± 0.082	18.537 ± 0.065	18.160 ± 0.094
587	21 40 29.13	58 18 04.83	18.675 ± 0.032	17.586 ± 0.016	17.150 ± 0.032
590	21 40 42.97	58 18 05.73	19.980 ± 0.112	18.416 ± 0.033	17.595 ± 0.046
591	21 40 24.27	58 18 06.18	19.499 ± 0.058	18.459 ± 0.044	18.042 ± 0.080
592	21 40 48.11	58 18 05.76	19.177 ± 0.049	17.831 ± 0.018	17.197 ± 0.030
593	21 40 31.16	58 18 07.35	19.226 ± 0.048	18.290 ± 0.029	17.847 ± 0.050
594	21 40 51.29	58 18 06.95	19.350 ± 0.059	17.837 ± 0.020	17.101 ± 0.028
596	21 40 46.81	58 18 07.34	19.098 ± 0.044	17.639 ± 0.018	16.913 ± 0.023
597	21 40 22.83	58 18 08.01	18.829 ± 0.031	17.981 ± 0.024	17.623 ± 0.052
598	21 40 34.08	58 18 08.39	15.644 ± 0.002	13.353 ± 0.001	12.254 ± 0.001
601	21 40 25.70	58 18 08.86	18.076 ± 0.025	17.409 ± 0.025	16.981 ± 0.070
604	21 40 49.19	58 18 09.83	19.435 ± 0.059	17.951 ± 0.020	17.131 ± 0.025
605	21 40 45.60	58 18 10.34	19.995 ± 0.094	18.494 ± 0.036	17.647 ± 0.045
606	21 40 27.86	58 18 10.50	18.371 ± 0.024	17.614 ± 0.016	17.212 ± 0.041
607	21 40 27.16	58 18 10.56	18.042 ± 0.018	17.106 ± 0.014	16.592 ± 0.026
609	21 40 21.99	58 18 11.10	18.965 ± 0.039	18.041 ± 0.032	17.595 ± 0.055
612	21 40 50.67	58 18 10.86	18.405 ± 0.026	17.393 ± 0.012	16.826 ± 0.019
613	21 40 22.35	58 18 11.97	18.386 ± 0.024	17.476 ± 0.017	17.151 ± 0.040
614	21 40 28.53	58 18 12.05	17.691 ± 0.011	16.648 ± 0.006	16.127 ± 0.013
616	21 40 31.27	58 18 12.47	17.130 ± 0.007	16.230 ± 0.004	15.738 ± 0.007
620	21 40 48.03	58 18 12.65	19.234 ± 0.050	17.905 ± 0.018	17.344 ± 0.033
621	21 40 22.96	58 18 13.29	18.654 ± 0.024	17.960 ± 0.026	17.580 ± 0.056
622	21 40 22.03	58 18 13.26	18.550 ± 0.027	17.896 ± 0.029	17.587 ± 0.062
625	21 40 50.51	58 18 14.23	18.427 ± 0.026	17.188 ± 0.011	16.612 ± 0.014
628	21 40 47.67	58 18 15.32	19.149 ± 0.050	17.998 ± 0.025	17.347 ± 0.034
629	21 40 51.90	58 18 16.00	19.163 ± 0.065	17.775 ± 0.025	17.226 ± 0.036
630	21 40 27.19	58 18 16.64	19.092 ± 0.053	18.192 ± 0.031	17.811 ± 0.087
632	21 40 41.94	58 18 16.53	17.975 ± 0.017	18.424 ± 0.033	18.220 ± 0.079
633	21 40 25.71	58 18 16.87	12.442 ± 0.026	11.508 ± 0.029	11.131 ± 0.019
634	21 40 24.33	58 18 16.96	18.438 ± 0.023	17.682 ± 0.020	17.441 ± 0.048
635	21 40 27.78	58 18 17.07	14.686 ± 0.001	13.722 ± 0.001	13.227 ± 0.001
636	21 40 29.70	58 18 17.35	18.996 ± 0.042	17.927 ± 0.025	17.379 ± 0.037
637	21 40 22.02	58 18 17.63	18.237 ± 0.020	17.619 ± 0.018	17.221 ± 0.039
638	21 40 47.93	58 18 17.34	18.783 ± 0.036	17.834 ± 0.022	17.307 ± 0.032
639	21 40 31.87	58 18 17.88	18.980 ± 0.035	17.751 ± 0.015	17.147 ± 0.027
640	21 40 26.89	58 18 18.47	17.444 ± 0.010	17.042 ± 0.011	16.631 ± 0.028
641	21 40 23.71	58 18 18.37	17.094 ± 0.006	16.566 ± 0.007	16.262 ± 0.018
642	21 40 28.08	58 18 18.59	18.641 ± 0.032	17.792 ± 0.023	17.314 ± 0.054
643	21 40 27.02	58 18 18.75	17.287 ± 0.009	16.681 ± 0.007	16.181 ± 0.018
644	21 40 30.62	58 18 18.91	18.037 ± 0.017	17.162 ± 0.009	16.683 ± 0.015
646	21 40 46.74	58 18 18.59	19.593 ± 0.067	18.328 ± 0.029	17.556 ± 0.042
647	21 40 26.18	58 18 19.64	19.577 ± 0.089	18.474 ± 0.046	17.765 ± 0.081
648	21 40 30.41	58 18 19.47	19.371 ± 0.057	18.294 ± 0.028	17.960 ± 0.054
650	21 40 25.61	58 18 20.73	17.410 ± 0.014	16.760 ± 0.010	16.310 ± 0.020
651	21 40 20.57	58 18 20.92	18.956 ± 0.045	17.746 ± 0.023	16.742 ± 0.025
652	21 40 50.97	58 18 20.81	18.774 ± 0.037	17.217 ± 0.010	16.663 ± 0.017
656	21 40 36.68	58 18 23.24	17.526 ± 0.011	15.139 ± 0.002	13.949 ± 0.002
657	21 40 30.30	58 18 24.87	19.070 ± 0.043	17.872 ± 0.018	17.490 ± 0.034
659	21 40 49.77	58 18 25.23	19.029 ± 0.043	17.747 ± 0.017	17.182 ± 0.023
660	21 40 40.45	58 18 26.37	18.364 ± 0.022	15.453 ± 0.003	13.834 ± 0.002
661	21 40 31.91	58 18 27.24	18.416 ± 0.022	17.131 ± 0.009	16.465 ± 0.015
662	21 40 28.33	58 18 27.25	14.557 ± 0.001	13.275 ± 0.001	12.635 ± 0.001
663	21 40 34.32	58 18 27.37	19.733 ± 0.070	17.211 ± 0.012	15.938 ± 0.010
664	21 40 29.40	58 18 28.29	17.115 ± 0.007	16.219 ± 0.004	15.656 ± 0.008
666	21 40 20.81	58 18 28.53	19.367 ± 0.060	18.445 ± 0.042	17.997 ± 0.080
667	21 40 47.52	58 18 28.25	18.625 ± 0.030	17.320 ± 0.014	16.595 ± 0.016
668	21 40 51.74	58 18 28.69	19.180 ± 0.064	17.815 ± 0.021	17.183 ± 0.038
669	21 40 25.67	58 18 29.91	18.017 ± 0.016	17.114 ± 0.011	16.475 ± 0.021
670	21 40 48.28	58 18 30.05	18.053 ± 0.019	17.045 ± 0.010	16.443 ± 0.016
671	21 40 36.19	58 18 31.08	19.880 ± 0.091	17.773 ± 0.017	16.692 ± 0.015
673	21 40 51.55	58 18 31.46	19.023 ± 0.047	17.825 ± 0.022	17.298 ± 0.044
674	21 40 35.27	58 18 32.24	17.202 ± 0.008	16.504 ± 0.006	16.101 ± 0.012
676	21 40 48.45	58 18 32.15	19.487 ± 0.075	18.098 ± 0.030	17.396 ± 0.038
678	21 40 25.47	58 18 33.31	16.751 ± 0.006	15.827 ± 0.004	15.147 ± 0.006
680	21 40 28.30	58 18 33.32	18.941 ± 0.037	17.777 ± 0.016	17.070 ± 0.040
682	21 40 29.39	58 18 33.94	19.229 ± 0.040	17.750 ± 0.016	17.098 ± 0.027

Table 1. Continued.

NIR source	α (J2000) ($^{\text{h}} \text{ m } \text{s}$)	δ (J2000) ($^{\circ} \text{ } '$ '')	J	H (mag)	K_s
684	21 40 46.61	58 18 33.91	18.499 \pm 0.027	16.861 \pm 0.007	15.992 \pm 0.011
686	21 40 39.86	58 18 35.03	18.324 \pm 0.021	15.116 \pm 0.002	13.288 \pm 0.001
688	21 40 27.01	58 18 35.49	19.881 \pm 0.090	18.465 \pm 0.031	17.759 \pm 0.063
690	21 40 30.42	58 18 36.30	18.993 \pm 0.041	17.644 \pm 0.018	17.142 \pm 0.024
691	21 40 48.48	58 18 36.48	18.372 \pm 0.024	17.051 \pm 0.009	16.367 \pm 0.014
693	21 40 23.08	58 18 37.52	16.618 \pm 0.005	15.893 \pm 0.004	15.553 \pm 0.009
694	21 40 21.51	58 18 38.71	18.957 \pm 0.039	18.229 \pm 0.034	17.943 \pm 0.079
696	21 40 46.62	58 18 39.40	20.554 \pm 0.166	18.430 \pm 0.035	17.652 \pm 0.051
698	21 40 46.96	58 18 40.85	18.310 \pm 0.025	17.134 \pm 0.011	16.491 \pm 0.016
699	21 40 30.76	58 18 41.39	12.853 \pm 0.027	12.203 \pm 0.032	12.079 \pm 0.026
700	21 40 27.75	58 18 42.11	18.558 \pm 0.025	17.702 \pm 0.015	17.005 \pm 0.031
701	21 40 22.99	58 18 41.95	19.404 \pm 0.060	18.498 \pm 0.051	17.917 \pm 0.085
702	21 40 33.32	58 18 42.73	19.449 \pm 0.065	17.999 \pm 0.021	17.072 \pm 0.031
703	21 40 43.36	58 18 42.83	16.269 \pm 0.004	14.407 \pm 0.001	13.480 \pm 0.001
705	21 40 20.33	58 18 43.73	17.310 \pm 0.014	16.591 \pm 0.010	16.120 \pm 0.014
707	21 40 47.79	58 18 43.43	19.046 \pm 0.046	17.491 \pm 0.015	16.787 \pm 0.018
708	21 40 22.90	58 18 44.24	17.997 \pm 0.018	16.561 \pm 0.010	15.987 \pm 0.015
709	21 40 46.75	58 18 44.04	19.304 \pm 0.062	17.673 \pm 0.017	16.973 \pm 0.025
710	21 40 21.67	58 18 44.61	14.688 \pm 0.001	13.791 \pm 0.001	13.420 \pm 0.001
711	21 40 50.21	58 18 44.35	16.887 \pm 0.009	16.062 \pm 0.004	15.611 \pm 0.005
712	21 40 29.75	58 18 44.97	18.387 \pm 0.026	17.169 \pm 0.011	16.539 \pm 0.017
716	21 40 25.24	58 18 45.56	19.382 \pm 0.064	18.067 \pm 0.027	17.252 \pm 0.040
717	21 40 20.64	58 18 46.23	17.751 \pm 0.016	16.814 \pm 0.010	16.378 \pm 0.018
718	21 40 28.47	58 18 46.11	15.128 \pm 0.002	14.323 \pm 0.001	13.702 \pm 0.002
719	21 40 51.38	58 18 46.04	16.698 \pm 0.008	15.603 \pm 0.003	15.045 \pm 0.005
720	21 40 27.16	58 18 47.70	18.221 \pm 0.025	17.137 \pm 0.012	16.503 \pm 0.023
721	21 40 34.54	58 18 47.84	19.085 \pm 0.044	17.724 \pm 0.014	16.949 \pm 0.023
722	21 40 25.89	58 18 49.10	19.390 \pm 0.074	18.092 \pm 0.025	17.165 \pm 0.036
723	21 40 27.63	58 18 49.38	15.165 \pm 0.002	14.483 \pm 0.001	14.092 \pm 0.002
726	21 40 48.09	58 18 49.67	18.613 \pm 0.044	17.178 \pm 0.012	16.411 \pm 0.014
727	21 40 28.42	58 18 51.23	18.000 \pm 0.024	16.913 \pm 0.010	16.276 \pm 0.019
730	21 40 50.06	58 18 52.49	12.490 \pm 0.027	11.538 \pm 0.028	11.144 \pm 0.021
731	21 40 45.91	58 18 52.46	16.687 \pm 0.007	15.425 \pm 0.003	14.846 \pm 0.004
732	21 40 44.19	58 18 52.92	16.180 \pm 0.005	15.008 \pm 0.002	14.356 \pm 0.002
735	21 40 29.40	58 18 53.36	18.984 \pm 0.049	17.582 \pm 0.017	16.952 \pm 0.025
737	21 40 46.37	58 18 53.47	19.036 \pm 0.061	18.061 \pm 0.032	17.605 \pm 0.050
738	21 40 22.20	58 18 54.08	15.676 \pm 0.003	15.059 \pm 0.002	14.665 \pm 0.004
740	21 40 28.53	58 18 55.24	17.744 \pm 0.016	16.742 \pm 0.008	16.181 \pm 0.015
744	21 40 45.56	58 18 55.74	17.030 \pm 0.010	16.268 \pm 0.006	15.800 \pm 0.009
745	21 40 44.76	58 18 56.32	18.772 \pm 0.045	17.660 \pm 0.021	17.116 \pm 0.028
746	21 40 27.16	58 18 56.65	19.766 \pm 0.104	18.488 \pm 0.051	17.688 \pm 0.066
749	21 40 51.85	58 18 57.64	18.160 \pm 0.037	17.314 \pm 0.025	16.626 \pm 0.022
750	21 40 44.07	58 18 57.78	16.598 \pm 0.007	15.092 \pm 0.002	14.344 \pm 0.002
752	21 40 27.74	58 18 58.90	17.753 \pm 0.018	16.836 \pm 0.011	16.214 \pm 0.017
753	21 40 49.29	58 18 58.42	18.285 \pm 0.028	17.567 \pm 0.023	16.977 \pm 0.021
757	21 40 32.32	58 19 00.51	15.243 \pm 0.002	14.691 \pm 0.002	14.358 \pm 0.002
758	21 40 23.33	58 19 01.40	19.668 \pm 0.115	18.422 \pm 0.054	17.742 \pm 0.063
759	21 40 30.06	58 19 01.51	17.136 \pm 0.010	16.586 \pm 0.010	16.114 \pm 0.009
760	21 40 33.06	58 19 01.70	19.289 \pm 0.074	18.336 \pm 0.046	17.591 \pm 0.042
764	21 40 31.78	58 19 02.87	18.685 \pm 0.054	17.195 \pm 0.019	16.332 \pm 0.012
765	21 40 29.26	58 19 03.19	18.915 \pm 0.067	17.820 \pm 0.034	17.499 \pm 0.043
842	21 40 51.42	58 15 18.14	19.001 \pm 0.039	18.329 \pm 0.031	18.009 \pm 0.107
843	21 40 49.55	58 15 11.31	19.184 \pm 0.046	18.259 \pm 0.026	18.422 \pm 0.085
844	21 40 48.90	58 15 15.21	19.822 \pm 0.090	17.866 \pm 0.020	18.038 \pm 0.075
846	21 40 47.20	58 15 12.13	19.724 \pm 0.072	18.967 \pm 0.057	18.584 \pm 0.120
847	21 40 46.12	58 15 16.43	19.233 \pm 0.050	18.328 \pm 0.029	17.960 \pm 0.081
848	21 40 44.39	58 15 06.71	20.467 \pm 0.154	18.498 \pm 0.037	18.391 \pm 0.085
854	21 40 47.17	58 15 26.54	20.056 \pm 0.117	19.018 \pm 0.069	18.670 \pm 0.144
892	21 40 51.07	58 16 28.68	19.717 \pm 0.078	18.786 \pm 0.049	18.246 \pm 0.088
893	21 40 50.31	58 16 28.33	20.042 \pm 0.111	18.635 \pm 0.045	18.151 \pm 0.068
894	21 40 49.56	58 16 25.34	19.956 \pm 0.091	18.818 \pm 0.055	18.046 \pm 0.064
897	21 40 47.66	58 15 47.57	20.248 \pm 0.113	19.075 \pm 0.047	18.902 \pm 0.130
899	21 40 41.80	58 14 55.51	18.964 \pm 0.067	17.823 \pm 0.034	17.713 \pm 0.112
900	21 40 41.06	58 15 05.68	19.423 \pm 0.105	18.517 \pm 0.056	18.096 \pm 0.109
901	21 40 42.09	58 15 06.65	19.641 \pm 0.083	18.143 \pm 0.033	17.590 \pm 0.057
903	21 40 40.05	58 15 28.75	19.632 \pm 0.058	18.450 \pm 0.032	17.815 \pm 0.058
906	21 40 36.92	58 15 19.57	19.345 \pm 0.081	18.243 \pm 0.040	17.985 \pm 0.103

Table 1. Continued.

NIR source	α (J2000) ($^{\text{h}} \text{ m } \text{s}$)	δ (J2000) ($^{\circ} \text{ } '$ '')	J	H (mag)	K_s
907	21 40 36.86	58 15 22.32	19.600 \pm 0.082	18.601 \pm 0.049	18.152 \pm 0.120
908	21 40 33.54	58 15 23.66	18.459 \pm 0.026	17.785 \pm 0.018	17.662 \pm 0.068
909	21 40 33.22	58 15 36.32	19.442 \pm 0.061	18.217 \pm 0.029	17.984 \pm 0.076
910	21 40 36.45	58 15 03.67	18.261 \pm 0.026	17.698 \pm 0.025	18.250 \pm 0.092
911	21 40 38.98	58 15 09.49	19.246 \pm 0.048	18.224 \pm 0.032	18.105 \pm 0.075
912	21 40 40.00	58 15 12.97	19.436 \pm 0.055	18.228 \pm 0.029	17.889 \pm 0.065
913	21 40 40.72	58 15 06.94	19.528 \pm 0.104	18.440 \pm 0.056	18.507 \pm 0.156
914	21 40 40.50	58 15 01.81	19.380 \pm 0.062	18.232 \pm 0.030	18.596 \pm 0.145
915	21 40 40.74	58 15 32.87	20.536 \pm 0.135	19.439 \pm 0.089	18.724 \pm 0.137
916	21 40 34.04	58 15 27.66	19.347 \pm 0.050	18.519 \pm 0.032	18.099 \pm 0.081
919	21 40 35.23	58 15 32.01	18.779 \pm 0.033	17.449 \pm 0.013	16.751 \pm 0.026
923	21 40 38.90	58 15 15.51	19.677 \pm 0.074	19.101 \pm 0.057	18.861 \pm 0.178
924	21 40 33.96	58 15 08.24	18.387 \pm 0.021	17.811 \pm 0.019	18.230 \pm 0.100
925	21 40 33.16	58 15 12.52	19.142 \pm 0.043	18.263 \pm 0.034	18.391 \pm 0.108
926	21 40 31.27	58 15 05.55	18.615 \pm 0.040	17.883 \pm 0.026	18.402 \pm 0.125
927	21 40 32.92	58 15 03.01	20.371 \pm 0.123	19.278 \pm 0.078	19.725 \pm 0.397
929	21 40 27.75	58 15 10.01	19.063 \pm 0.051	18.353 \pm 0.039	17.860 \pm 0.094
930	21 40 26.26	58 15 14.05	18.898 \pm 0.037	18.029 \pm 0.024	17.912 \pm 0.101
931	21 40 26.87	58 15 28.95	19.398 \pm 0.053	18.478 \pm 0.030	18.210 \pm 0.125
932	21 40 26.73	58 15 32.08	19.095 \pm 0.042	18.510 \pm 0.035	18.302 \pm 0.137
933	21 40 26.47	58 15 34.97	18.818 \pm 0.031	18.279 \pm 0.026	17.872 \pm 0.081
934	21 40 26.87	58 15 37.22	19.598 \pm 0.058	18.663 \pm 0.038	18.262 \pm 0.117
935	21 40 27.39	58 15 35.58	19.523 \pm 0.059	18.602 \pm 0.034	18.171 \pm 0.120
936	21 40 27.66	58 15 37.95	19.334 \pm 0.055	18.414 \pm 0.026	18.057 \pm 0.103
937	21 40 29.98	58 15 07.21	18.608 \pm 0.030	18.016 \pm 0.023	18.642 \pm 0.132
938	21 40 30.48	58 15 22.86	18.687 \pm 0.030	18.512 \pm 0.037	19.236 \pm 0.186
939	21 40 32.99	58 15 32.73	17.994 \pm 0.014	17.448 \pm 0.012	17.148 \pm 0.035
940	21 40 28.33	58 15 31.70	18.761 \pm 0.030	17.840 \pm 0.016	17.415 \pm 0.061
941	21 40 27.48	58 15 09.52	18.867 \pm 0.037	17.925 \pm 0.021	17.450 \pm 0.063
949	21 40 27.99	58 15 57.36	19.213 \pm 0.045	18.258 \pm 0.031	17.993 \pm 0.088
950	21 40 30.83	58 15 57.42	19.664 \pm 0.068	18.589 \pm 0.041	18.355 \pm 0.086
951	21 40 28.18	58 16 05.62	19.656 \pm 0.064	18.792 \pm 0.048	18.616 \pm 0.155
952	21 40 31.74	58 15 57.28	19.468 \pm 0.053	18.021 \pm 0.020	17.345 \pm 0.034
953	21 40 30.93	58 16 00.91	18.598 \pm 0.028	17.711 \pm 0.017	17.437 \pm 0.039
954	21 40 31.85	58 15 43.08	19.467 \pm 0.067	18.315 \pm 0.051	17.794 \pm 0.080
955	21 40 27.94	58 15 53.22	18.314 \pm 0.020	17.687 \pm 0.017	17.369 \pm 0.053
956	21 40 31.60	58 15 47.01	20.162 \pm 0.104	19.068 \pm 0.066	19.100 \pm 0.221
957	21 40 31.89	58 16 21.23	20.114 \pm 0.122	18.273 \pm 0.029	17.350 \pm 0.038
958	21 40 24.68	58 15 54.73	18.562 \pm 0.028	17.733 \pm 0.019	17.360 \pm 0.048
959	21 40 25.50	58 15 50.96	18.832 \pm 0.042	17.918 \pm 0.030	17.605 \pm 0.064
960	21 40 23.38	58 15 31.91	17.679 \pm 0.014	16.763 \pm 0.011	16.457 \pm 0.025
961	21 40 21.01	58 15 32.20	19.866 \pm 0.089	18.323 \pm 0.043	17.250 \pm 0.051
965	21 40 31.54	58 16 16.70	20.958 \pm 0.272	19.098 \pm 0.061	18.441 \pm 0.090
966	21 40 29.91	58 16 23.37	19.650 \pm 0.074	18.391 \pm 0.029	18.083 \pm 0.066
967	21 40 28.07	58 16 26.55	19.104 \pm 0.042	18.407 \pm 0.029	18.064 \pm 0.073
968	21 40 27.30	58 16 17.67	19.071 \pm 0.040	18.076 \pm 0.022	17.856 \pm 0.067
969	21 40 25.75	58 15 56.28	19.510 \pm 0.061	18.814 \pm 0.048	18.260 \pm 0.103
970	21 40 26.08	58 15 51.01	19.735 \pm 0.084	18.836 \pm 0.047	18.479 \pm 0.133
971	21 40 25.16	58 16 21.22	19.152 \pm 0.047	18.332 \pm 0.033	18.024 \pm 0.093
972	21 40 24.86	58 16 24.86	19.842 \pm 0.080	18.809 \pm 0.047	18.268 \pm 0.103
973	21 40 28.82	58 16 23.04	19.057 \pm 0.042	18.182 \pm 0.024	17.794 \pm 0.070
974	21 40 25.33	58 16 11.05	18.684 \pm 0.047	17.860 \pm 0.033	17.526 \pm 0.073
975	21 40 24.26	58 15 17.10	18.800 \pm 0.030	18.128 \pm 0.030	17.895 \pm 0.098
976	21 40 23.72	58 15 12.35	19.579 \pm 0.071	18.973 \pm 0.086	18.469 \pm 0.159
977	21 40 21.74	58 15 13.52	18.333 \pm 0.024	17.545 \pm 0.024	17.427 \pm 0.063
978	21 40 21.12	58 15 27.31	19.471 \pm 0.077	18.472 \pm 0.049	18.234 \pm 0.155
982	21 40 20.77	58 15 20.92	18.947 \pm 0.044	17.980 \pm 0.030	17.702 \pm 0.092
983	21 40 25.22	58 15 41.26	19.585 \pm 0.078	18.766 \pm 0.052	18.420 \pm 0.141
984	21 40 23.91	58 15 21.87	19.213 \pm 0.049	18.310 \pm 0.043	18.096 \pm 0.132
988	21 40 23.92	58 15 29.51	19.237 \pm 0.059	18.709 \pm 0.057	18.160 \pm 0.121
989	21 40 20.91	58 14 58.78	17.145 \pm 0.009	16.598 \pm 0.010	17.507 \pm 0.048
996	21 40 23.07	58 16 08.73	20.172 \pm 0.124	19.140 \pm 0.088	18.471 \pm 0.135
997	21 40 25.28	58 15 57.67	20.551 \pm 0.164	19.492 \pm 0.091	18.616 \pm 0.126
998	21 40 23.83	58 16 00.95	20.522 \pm 0.149	19.482 \pm 0.101	18.571 \pm 0.138
999	21 40 23.07	58 15 56.21	20.214 \pm 0.111	19.264 \pm 0.090	18.458 \pm 0.120
1003	21 40 19.95	58 15 42.61	19.908 \pm 0.112	19.033 \pm 0.102	18.989 \pm 0.260
1004	21 40 20.15	58 15 54.01	19.337 \pm 0.064	18.374 \pm 0.050	18.235 \pm 0.110

Table 1. Continued.

NIR source	α (J2000) ($^{\text{h}} \text{ m } \text{s}$)	δ (J2000) ($^{\circ} \text{ } '$ '')	J	H (mag)	K_s
1005	21 40 22.87	58 16 04.10	19.463 \pm 0.064	18.380 \pm 0.042	17.981 \pm 0.085
1007	21 40 23.78	58 15 45.02	19.502 \pm 0.068	18.350 \pm 0.042	17.924 \pm 0.085
1008	21 40 23.51	58 15 43.79	18.868 \pm 0.037	17.958 \pm 0.029	17.518 \pm 0.069
1009	21 40 21.08	58 15 44.97	18.143 \pm 0.028	17.618 \pm 0.033	16.964 \pm 0.040
1010	21 40 22.01	58 15 48.12	19.413 \pm 0.059	18.414 \pm 0.042	17.866 \pm 0.074
1011	21 40 22.26	58 15 56.23	18.917 \pm 0.033	18.028 \pm 0.030	17.465 \pm 0.054
1012	21 40 21.92	58 15 59.92	19.484 \pm 0.062	18.374 \pm 0.043	17.921 \pm 0.081
1013	21 40 20.64	58 15 56.79	18.882 \pm 0.047	18.118 \pm 0.043	17.555 \pm 0.056
1014	21 40 23.02	58 16 01.87	19.251 \pm 0.053	18.267 \pm 0.033	17.875 \pm 0.080
1015	21 40 20.86	58 15 53.62	19.369 \pm 0.081	18.246 \pm 0.054	17.794 \pm 0.080
1016	21 40 23.35	58 15 41.92	19.735 \pm 0.081	18.682 \pm 0.061	18.006 \pm 0.101
1017	21 40 19.62	58 15 51.38	18.818 \pm 0.069	17.765 \pm 0.038	17.586 \pm 0.064
1019	21 40 20.86	58 15 42.22	18.819 \pm 0.047	18.115 \pm 0.049	17.620 \pm 0.073
1027	21 40 46.88	58 16 33.57	18.365 \pm 0.022	18.620 \pm 0.044	18.991 \pm 0.190
1035	21 40 45.81	58 16 21.83	20.828 \pm 0.219	18.964 \pm 0.080	18.053 \pm 0.114
1060	21 40 50.46	58 17 16.55	20.312 \pm 0.144	19.592 \pm 0.109	18.432 \pm 0.101
1063	21 40 41.32	58 17 18.45	19.158 \pm 0.048	17.967 \pm 0.026	18.615 \pm 0.136
1069	21 40 46.68	58 17 29.82	18.577 \pm 0.028	18.654 \pm 0.043	19.108 \pm 0.215
1084	21 40 37.32	58 16 50.84	20.787 \pm 0.240	19.048 \pm 0.065	18.101 \pm 0.067
1086	21 40 31.42	58 16 38.62	20.814 \pm 0.235	18.794 \pm 0.054	18.041 \pm 0.070
1087	21 40 26.61	58 16 39.23	19.323 \pm 0.060	18.288 \pm 0.029	17.918 \pm 0.085
1088	21 40 28.06	58 16 50.97	19.581 \pm 0.077	18.556 \pm 0.048	18.090 \pm 0.122
1089	21 40 27.36	58 16 47.48	20.306 \pm 0.137	19.296 \pm 0.073	18.744 \pm 0.177
1090	21 40 28.78	58 16 52.34	19.327 \pm 0.063	18.554 \pm 0.041	18.183 \pm 0.142
1091	21 40 30.49	58 16 44.78	20.583 \pm 0.205	19.507 \pm 0.110	18.889 \pm 0.143
1092	21 40 29.77	58 16 45.17	21.770 \pm 0.606	19.642 \pm 0.122	18.932 \pm 0.177
1094	21 40 24.22	58 16 25.87	19.193 \pm 0.040	18.427 \pm 0.034	18.204 \pm 0.095
1095	21 40 24.04	58 16 45.17	19.435 \pm 0.060	18.517 \pm 0.042	18.138 \pm 0.092
1096	21 40 23.36	58 16 49.94	19.822 \pm 0.088	18.672 \pm 0.055	17.874 \pm 0.082
1097	21 40 22.29	58 16 38.06	19.390 \pm 0.057	18.517 \pm 0.044	18.197 \pm 0.106
1098	21 40 22.05	58 16 38.94	19.510 \pm 0.066	18.602 \pm 0.053	18.034 \pm 0.102
1099	21 40 21.71	58 16 40.95	19.312 \pm 0.052	18.442 \pm 0.044	18.293 \pm 0.120
1100	21 40 21.91	58 16 40.57	20.170 \pm 0.117	19.583 \pm 0.125	18.690 \pm 0.181
1101	21 40 21.23	58 16 45.35	20.453 \pm 0.156	19.120 \pm 0.075	19.072 \pm 0.233
1102	21 40 22.15	58 16 52.47	20.030 \pm 0.098	18.939 \pm 0.072	18.513 \pm 0.128
1103	21 40 20.39	58 16 33.21	19.316 \pm 0.060	18.705 \pm 0.056	18.228 \pm 0.115
1104	21 40 19.59	58 16 38.61	19.462 \pm 0.136	18.442 \pm 0.062	18.034 \pm 0.088
1108	21 40 20.40	58 16 19.31	19.558 \pm 0.079	18.943 \pm 0.074	18.652 \pm 0.159
1109	21 40 22.99	58 16 30.28	19.059 \pm 0.046	18.404 \pm 0.045	18.221 \pm 0.109
1110	21 40 25.85	58 16 34.99	20.779 \pm 0.228	19.460 \pm 0.080	19.402 \pm 0.282
1111	21 40 25.66	58 16 39.50	20.000 \pm 0.109	18.940 \pm 0.049	18.816 \pm 0.169
1112	21 40 19.69	58 16 31.85	18.966 \pm 0.085	18.333 \pm 0.057	17.796 \pm 0.082
1115	21 40 25.16	58 16 32.63	19.190 \pm 0.046	18.136 \pm 0.020	17.663 \pm 0.055
1116	21 40 23.69	58 16 24.56	19.161 \pm 0.043	18.342 \pm 0.036	17.878 \pm 0.075
1117	21 40 23.61	58 16 26.54	19.131 \pm 0.046	18.226 \pm 0.037	17.965 \pm 0.084
1118	21 40 21.39	58 16 42.70	19.011 \pm 0.038	18.040 \pm 0.028	17.710 \pm 0.060
1121	21 40 25.55	58 16 35.88	19.042 \pm 0.044	18.171 \pm 0.023	17.563 \pm 0.049
1124	21 40 37.82	58 17 07.78	20.386 \pm 0.162	18.627 \pm 0.045	17.889 \pm 0.062
1126	21 40 36.22	58 17 21.60	19.273 \pm 0.061	18.610 \pm 0.042	18.253 \pm 0.093
1132	21 40 34.03	58 17 17.64	20.002 \pm 0.116	18.629 \pm 0.037	17.992 \pm 0.068
1133	21 40 33.34	58 17 16.28	20.690 \pm 0.239	18.995 \pm 0.058	18.473 \pm 0.113
1134	21 40 30.78	58 17 06.45	19.698 \pm 0.093	18.561 \pm 0.036	18.317 \pm 0.083
1135	21 40 30.46	58 17 00.69	19.708 \pm 0.096	18.621 \pm 0.039	18.307 \pm 0.082
1136	21 40 26.83	58 16 59.64	18.976 \pm 0.039	18.271 \pm 0.024	17.992 \pm 0.086
1137	21 40 26.44	58 16 55.14	19.613 \pm 0.075	18.964 \pm 0.045	18.597 \pm 0.148
1138	21 40 23.79	58 16 56.32	18.923 \pm 0.037	18.183 \pm 0.037	18.016 \pm 0.104
1139	21 40 25.45	58 17 01.80	19.264 \pm 0.050	18.631 \pm 0.043	18.319 \pm 0.117
1140	21 40 24.07	58 17 07.09	19.259 \pm 0.049	18.259 \pm 0.043	17.929 \pm 0.096
1142	21 40 22.84	58 17 05.11	19.525 \pm 0.064	18.594 \pm 0.055	18.212 \pm 0.121
1143	21 40 23.07	58 17 07.49	19.268 \pm 0.046	18.354 \pm 0.037	17.879 \pm 0.092
1144	21 40 23.48	58 17 02.09	19.993 \pm 0.087	19.043 \pm 0.067	18.603 \pm 0.160
1146	21 40 21.35	58 17 11.40	19.373 \pm 0.049	18.646 \pm 0.047	18.285 \pm 0.120
1147	21 40 22.24	58 17 16.90	19.570 \pm 0.057	18.489 \pm 0.037	17.983 \pm 0.090
1148	21 40 23.26	58 17 15.25	19.876 \pm 0.081	19.053 \pm 0.067	18.252 \pm 0.110
1226	21 40 51.37	58 18 36.19	19.753 \pm 0.098	18.576 \pm 0.040	18.221 \pm 0.096
1227	21 40 50.80	58 18 39.34	20.292 \pm 0.151	19.150 \pm 0.061	18.659 \pm 0.104
1228	21 40 50.97	58 18 58.75	19.243 \pm 0.056	18.659 \pm 0.070	18.414 \pm 0.090

Table 1. Continued.

NIR source	α (J2000) ($^{\text{h}} \text{ m } \text{s}$)	δ (J2000) ($^{\circ} \text{ } '$ '')	J	H (mag)	K_s
1232	21 40 48.32	58 18 59.47	19.623 ± 0.106	18.727 ± 0.075	19.020 ± 0.189
1234	21 40 46.75	58 18 36.71	20.284 ± 0.135	18.904 ± 0.053	18.207 ± 0.080
1235	21 40 48.25	58 18 34.91	20.382 ± 0.156	19.008 ± 0.059	18.359 ± 0.100
1237	21 40 49.53	58 18 35.63	20.331 ± 0.142	19.053 ± 0.058	18.891 ± 0.121
1245	21 40 52.25	58 18 24.89	19.084 ± 0.098	18.316 ± 0.036	17.797 ± 0.066
1246	21 40 50.89	58 18 29.94	20.190 ± 0.123	18.911 ± 0.056	18.494 ± 0.097
1247	21 40 49.22	58 18 48.16	19.763 ± 0.100	19.080 ± 0.066	18.516 ± 0.087
1251	21 40 47.50	58 18 21.91	19.769 ± 0.094	18.914 ± 0.057	18.152 ± 0.073
1253	21 40 47.60	58 18 08.75	19.626 ± 0.076	18.440 ± 0.035	17.744 ± 0.048
1254	21 40 47.95	58 18 02.35	20.646 ± 0.184	18.798 ± 0.051	18.090 ± 0.077
1255	21 40 47.92	58 17 59.35	20.490 ± 0.169	19.372 ± 0.084	18.935 ± 0.166
1259	21 40 48.57	58 18 11.60	20.777 ± 0.195	18.981 ± 0.056	18.506 ± 0.091
1260	21 40 48.91	58 17 50.30	20.096 ± 0.116	18.621 ± 0.039	18.031 ± 0.074
1273	21 40 43.77	58 18 53.59	19.810 ± 0.117	18.875 ± 0.068	18.450 ± 0.093
1277	21 40 45.79	58 18 57.04	19.841 ± 0.127	18.546 ± 0.055	18.009 ± 0.072
1295	21 40 35.85	58 18 53.43	20.035 ± 0.156	18.510 ± 0.041	17.873 ± 0.052
1297	21 40 35.19	58 18 37.04	20.411 ± 0.149	18.874 ± 0.059	18.036 ± 0.065
1298	21 40 35.12	58 18 41.92	20.195 ± 0.127	18.725 ± 0.044	17.810 ± 0.049
1300	21 40 37.22	58 18 36.80	18.979 ± 0.039	18.233 ± 0.029	17.805 ± 0.051
1305	21 40 36.36	58 17 47.90	21.130 ± 0.284	19.029 ± 0.057	18.267 ± 0.081
1307	21 40 37.10	58 17 40.74	20.161 ± 0.119	18.642 ± 0.039	17.661 ± 0.053
1308	21 40 36.23	58 17 44.65	20.440 ± 0.152	18.820 ± 0.043	18.047 ± 0.070
1310	21 40 33.53	58 17 33.44	19.457 ± 0.068	18.603 ± 0.040	18.047 ± 0.070
1311	21 40 32.46	58 17 37.85	19.838 ± 0.092	18.753 ± 0.051	18.392 ± 0.102
1312	21 40 32.15	58 17 36.23	20.037 ± 0.117	18.930 ± 0.053	18.443 ± 0.102
1313	21 40 32.25	58 17 29.21	19.832 ± 0.115	18.906 ± 0.072	18.533 ± 0.133
1314	21 40 31.63	58 17 18.83	20.029 ± 0.126	18.594 ± 0.039	17.960 ± 0.065
1315	21 40 33.78	58 17 22.03	19.805 ± 0.107	18.634 ± 0.046	18.072 ± 0.088
1316	21 40 35.70	58 17 30.51	19.994 ± 0.107	18.933 ± 0.046	18.271 ± 0.084
1317	21 40 30.41	58 17 33.51	20.045 ± 0.092	18.860 ± 0.064	18.323 ± 0.098
1318	21 40 30.03	58 17 27.13	20.132 ± 0.098	18.838 ± 0.051	18.024 ± 0.071
1319	21 40 30.48	58 17 30.51	18.636 ± 0.025	18.348 ± 0.032	18.758 ± 0.125
1320	21 40 29.94	58 17 38.79	19.640 ± 0.059	18.736 ± 0.035	18.318 ± 0.106
1321	21 40 35.04	58 17 32.29	20.007 ± 0.115	18.538 ± 0.034	17.598 ± 0.046
1323	21 40 34.23	58 17 50.08	20.910 ± 0.234	18.913 ± 0.047	18.256 ± 0.102
1325	21 40 32.29	58 17 47.37	19.730 ± 0.081	18.672 ± 0.044	18.165 ± 0.100
1326	21 40 31.79	58 17 45.38	20.057 ± 0.087	18.871 ± 0.047	18.427 ± 0.098
1327	21 40 32.09	58 17 51.64	19.749 ± 0.074	18.765 ± 0.049	18.217 ± 0.098
1328	21 40 29.80	58 18 12.74	20.159 ± 0.138	18.763 ± 0.058	18.326 ± 0.089
1331	21 40 30.50	58 18 26.63	20.504 ± 0.162	18.964 ± 0.051	18.591 ± 0.088
1334	21 40 30.73	58 18 02.57	20.088 ± 0.094	19.053 ± 0.051	18.710 ± 0.099
1341	21 40 30.03	58 18 44.17	21.060 ± 0.283	18.818 ± 0.055	18.076 ± 0.064
1343	21 40 31.60	58 18 55.91	19.847 ± 0.100	18.741 ± 0.049	18.077 ± 0.062
1344	21 40 32.28	58 19 03.54	19.875 ± 0.286	18.421 ± 0.075	17.766 ± 0.056
1345	21 40 29.87	58 19 00.46	19.072 ± 0.059	18.403 ± 0.052	17.881 ± 0.055
1346	21 40 29.72	58 18 58.71	19.513 ± 0.083	18.515 ± 0.049	18.203 ± 0.079
1355	21 40 24.73	58 19 00.20	19.884 ± 0.129	18.667 ± 0.061	17.988 ± 0.080
1356	21 40 25.39	58 18 49.66	20.109 ± 0.149	19.386 ± 0.092	18.258 ± 0.098
1357	21 40 26.60	58 18 41.87	20.123 ± 0.121	18.777 ± 0.048	17.913 ± 0.080
1360	21 40 28.37	58 18 58.62	20.375 ± 0.161	18.921 ± 0.070	18.378 ± 0.122
1365	21 40 27.21	58 18 46.49	19.333 ± 0.069	18.273 ± 0.036	18.079 ± 0.100
1366	21 40 28.68	58 18 33.56	20.358 ± 0.130	18.742 ± 0.037	17.934 ± 0.077
1367	21 40 29.34	58 18 25.15	19.322 ± 0.052	18.319 ± 0.032	17.815 ± 0.064
1368	21 40 29.00	58 18 19.90	20.243 ± 0.124	18.927 ± 0.051	18.332 ± 0.101
1369	21 40 29.26	58 18 15.13	19.898 ± 0.104	18.877 ± 0.065	18.623 ± 0.125
1370	21 40 28.53	58 18 20.78	19.962 ± 0.094	18.823 ± 0.048	18.165 ± 0.098
1373	21 40 27.42	58 18 33.33	19.919 ± 0.085	18.764 ± 0.039	18.185 ± 0.090
1375	21 40 26.77	58 18 31.59	20.220 ± 0.111	19.108 ± 0.058	18.417 ± 0.117
1376	21 40 27.15	58 18 24.70	19.920 ± 0.084	18.959 ± 0.046	18.556 ± 0.149
1378	21 40 25.40	58 18 30.12	20.544 ± 0.177	18.825 ± 0.064	18.246 ± 0.120
1379	21 40 25.54	58 18 24.48	20.130 ± 0.109	18.969 ± 0.058	18.334 ± 0.116
1380	21 40 25.51	58 18 14.21	18.115 ± 0.027	17.584 ± 0.021	17.814 ± 0.118
1381	21 40 25.08	58 18 14.22	20.201 ± 0.183	19.014 ± 0.106	18.392 ± 0.170
1382	21 40 24.82	58 18 10.84	19.146 ± 0.057	18.447 ± 0.049	18.323 ± 0.116
1383	21 40 26.70	58 18 09.42	19.464 ± 0.102	18.503 ± 0.069	18.337 ± 0.183
1384	21 40 24.46	58 18 13.73	19.930 ± 0.097	18.945 ± 0.069	18.609 ± 0.138
1385	21 40 23.85	58 18 11.61	19.940 ± 0.082	18.673 ± 0.049	18.222 ± 0.099

Table 1. Continued.

NIR source	α (J2000) ($^{\text{h}} \text{ m } \text{s}$)	δ (J2000) ($^{\circ} \text{ } '$ '')	J	H (mag)	K_s
1386	21 40 24.24	58 18 31.27	19.845 \pm 0.079	18.669 \pm 0.052	18.151 \pm 0.091
1387	21 40 26.53	58 17 48.63	19.360 \pm 0.063	18.414 \pm 0.041	17.865 \pm 0.069
1388	21 40 28.65	58 17 36.68	19.972 \pm 0.093	18.458 \pm 0.032	17.735 \pm 0.074
1389	21 40 29.40	58 17 31.53	20.199 \pm 0.108	18.865 \pm 0.055	18.246 \pm 0.119
1390	21 40 22.61	58 17 48.71	19.914 \pm 0.100	19.087 \pm 0.072	18.613 \pm 0.153
1391	21 40 22.21	58 17 47.09	19.601 \pm 0.067	18.643 \pm 0.048	18.013 \pm 0.091
1393	21 40 23.75	58 17 39.67	20.183 \pm 0.125	18.904 \pm 0.066	18.471 \pm 0.114
1395	21 40 23.74	58 17 25.89	19.351 \pm 0.082	18.399 \pm 0.066	17.905 \pm 0.089
1396	21 40 27.04	58 17 26.82	19.518 \pm 0.059	18.700 \pm 0.038	18.406 \pm 0.149
1397	21 40 26.12	58 17 27.84	19.830 \pm 0.073	18.881 \pm 0.042	18.417 \pm 0.124
1401	21 40 20.15	58 17 24.58	19.597 \pm 0.086	18.620 \pm 0.058	18.333 \pm 0.101
1404	21 40 20.08	58 17 18.19	19.586 \pm 0.088	18.754 \pm 0.068	18.336 \pm 0.107
1405	21 40 20.91	58 17 18.05	19.334 \pm 0.045	18.621 \pm 0.048	18.089 \pm 0.097
1406	21 40 21.04	58 17 22.31	19.007 \pm 0.037	18.253 \pm 0.034	18.001 \pm 0.079
1407	21 40 20.98	58 17 29.07	20.211 \pm 0.111	19.235 \pm 0.080	19.068 \pm 0.196
1408	21 40 21.35	58 17 35.65	18.803 \pm 0.041	17.896 \pm 0.043	17.110 \pm 0.045
1410	21 40 20.74	58 18 05.03	19.565 \pm 0.067	18.645 \pm 0.052	18.636 \pm 0.154
1415	21 40 20.46	58 18 19.19	19.744 \pm 0.092	18.601 \pm 0.052	18.330 \pm 0.108
1419	21 40 20.97	58 18 35.09	19.469 \pm 0.057	18.512 \pm 0.040	18.132 \pm 0.090
1427	21 40 25.53	58 17 59.42	19.053 \pm 0.107	18.452 \pm 0.149	17.337 \pm 0.080
1429	21 40 31.60	58 17 48.77	20.380 \pm 0.134	19.306 \pm 0.069	18.692 \pm 0.128
1430	21 40 31.02	58 17 48.78	20.778 \pm 0.163	19.364 \pm 0.064	19.342 \pm 0.233
1431	21 40 33.98	58 17 51.47	20.112 \pm 0.107	19.407 \pm 0.086	18.578 \pm 0.145
1433	21 40 26.72	58 18 19.69	19.757 \pm 0.080	19.002 \pm 0.058	18.353 \pm 0.120
1434	21 40 26.82	58 18 27.96	20.240 \pm 0.113	19.259 \pm 0.072	18.795 \pm 0.178
1436	21 40 29.33	58 18 45.94	20.139 \pm 0.140	19.205 \pm 0.073	19.154 \pm 0.208
1437	21 40 24.94	58 18 20.73	19.844 \pm 0.112	18.994 \pm 0.071	18.593 \pm 0.149
1438	21 40 24.81	58 18 20.99	20.378 \pm 0.161	19.050 \pm 0.073	18.448 \pm 0.128
1441	21 40 30.45	58 17 41.78	20.024 \pm 0.087	19.291 \pm 0.066	19.360 \pm 0.237
1442	21 40 30.42	58 17 44.04	20.426 \pm 0.119	19.582 \pm 0.081	19.135 \pm 0.218
1444	21 40 30.07	58 17 49.05	20.141 \pm 0.092	19.158 \pm 0.056	19.198 \pm 0.219
1445	21 40 23.37	58 18 03.73	19.966 \pm 0.097	18.673 \pm 0.052	18.401 \pm 0.123
1446	21 40 24.96	58 17 52.92	20.245 \pm 0.159	19.140 \pm 0.094	18.524 \pm 0.144
1453	21 40 51.80	58 17 44.44	20.693 \pm 0.288	19.299 \pm 0.093	18.605 \pm 0.183
1456	21 40 50.38	58 19 01.40	20.137 \pm 0.213	18.834 \pm 0.091	18.658 \pm 0.092
1458	21 40 43.60	58 16 12.54	18.537 \pm 0.033	17.623 \pm 0.040	16.369 \pm 0.057
1459	21 40 46.84	58 16 15.29	19.949 \pm 0.085	18.745 \pm 0.048	17.632 \pm 0.045
1467	21 40 40.40	58 15 59.41	18.875 \pm 0.033	17.713 \pm 0.026	16.727 \pm 0.045
1468	21 40 29.84	58 17 20.75	20.174 \pm 0.116	19.145 \pm 0.065	18.804 \pm 0.169
1469	21 40 28.82	58 17 26.03	20.499 \pm 0.135	19.701 \pm 0.100	18.693 \pm 0.178
1470	21 40 27.23	58 17 27.32	19.731 \pm 0.079	18.949 \pm 0.051	19.175 \pm 0.321
1471	21 40 27.36	58 17 28.57	20.556 \pm 0.234	19.189 \pm 0.090	18.982 \pm 0.243
1472	21 40 27.65	58 17 30.82	20.231 \pm 0.209	19.058 \pm 0.110	18.809 \pm 0.256
1473	21 40 27.87	58 17 32.32	20.827 \pm 0.229	19.744 \pm 0.123	18.909 \pm 0.235
1474	21 40 26.89	58 17 34.84	19.885 \pm 0.150	19.311 \pm 0.121	18.640 \pm 0.173
1475	21 40 32.94	58 17 09.90	20.853 \pm 0.244	19.492 \pm 0.102	19.218 \pm 0.259
1477	21 40 30.82	58 16 04.81	19.975 \pm 0.095	19.056 \pm 0.050	18.768 \pm 0.096
1478	21 40 30.53	58 16 09.83	19.763 \pm 0.080	18.900 \pm 0.054	18.467 \pm 0.079
1479	21 40 33.36	58 17 26.18	20.290 \pm 0.223	19.183 \pm 0.087	18.916 \pm 0.178
1480	21 40 25.30	58 17 32.62	19.956 \pm 0.110	19.230 \pm 0.085	18.639 \pm 0.207
1481	21 40 27.57	58 16 44.22	19.985 \pm 0.137	19.350 \pm 0.126	19.559 \pm 0.499
1482	21 40 29.39	58 16 06.10	20.047 \pm 0.085	19.161 \pm 0.060	19.018 \pm 0.150
1483	21 40 30.22	58 16 14.60	20.392 \pm 0.154	19.175 \pm 0.064	19.154 \pm 0.172
1484	21 40 28.88	58 17 02.73	18.979 \pm 0.035	17.877 \pm 0.019	17.989 \pm 0.115
1485	21 40 33.30	58 15 14.40	19.660 \pm 0.071	18.706 \pm 0.048	18.968 \pm 0.176
1486	21 40 34.13	58 15 13.62	19.680 \pm 0.076	18.712 \pm 0.043	18.884 \pm 0.174
1487	21 40 33.41	58 15 36.69	19.810 \pm 0.099	18.745 \pm 0.056	18.252 \pm 0.110
1488	21 40 32.76	58 15 00.88	20.299 \pm 0.138	19.000 \pm 0.073	19.388 \pm 0.269
1490	21 40 35.83	58 14 57.30	18.656 \pm 0.034	18.052 \pm 0.023	18.864 \pm 0.204
1491	21 40 25.08	58 15 15.83	19.505 \pm 0.064	18.521 \pm 0.041	18.245 \pm 0.136
1492	21 40 24.80	58 15 17.84	20.051 \pm 0.095	19.016 \pm 0.068	18.477 \pm 0.168
1493	21 40 31.28	58 15 29.23	20.385 \pm 0.120	19.103 \pm 0.055	18.806 \pm 0.138
1496	21 40 43.55	58 15 18.88	20.022 \pm 0.083	18.695 \pm 0.036	17.805 \pm 0.062

(a) The source # 331 is double (see Sect. 3.1). The two components have been labeled A and B. The source # 331A has been detected in the 3 bands and # 331B in the H and K_s bands only.

Table 2. JHK_s photometry and positions of found K_s sources detected in the H and K_s bands.

NIR source	α (J2000) ($^{\text{h}} \text{ m} \text{ s}$)	δ (J2000) ($^{\circ} \text{ ' } \text{ ''}$)	J	H (mag)	K_s
95	21 40 44.61	58 15 21.62	>20.860	18.819 \pm 0.043	17.613 \pm 0.053
144	21 40 38.20	58 15 33.09	>20.874	18.318 \pm 0.032	16.723 \pm 0.023
162	21 40 45.20	58 15 36.91	>20.842	19.402 \pm 0.075	17.456 \pm 0.036
206	21 40 46.50	58 15 51.78	>20.841	19.455 \pm 0.088	17.492 \pm 0.036
231	21 40 50.56	58 16 02.03	>20.835	19.646 \pm 0.100	17.553 \pm 0.032
252	21 40 40.97	58 16 12.32	>20.921	16.670 \pm 0.013	13.840 \pm 0.003
254	21 40 50.90	58 16 12.48	>20.865	18.643 \pm 0.038	17.417 \pm 0.031
255	21 40 33.68	58 16 13.18	>20.871	18.451 \pm 0.031	17.056 \pm 0.024
264	21 40 38.17	58 16 16.63	>20.843	19.404 \pm 0.099	18.056 \pm 0.065
271	21 40 43.62	58 16 19.11	>20.881	17.972 \pm 0.031	13.910 \pm 0.003
274	21 40 34.38	58 16 19.44	>20.880	18.117 \pm 0.026	16.680 \pm 0.017
276	21 40 48.61	58 16 19.71	>20.873	18.390 \pm 0.044	17.290 \pm 0.038
302	21 40 36.47	58 16 28.96	>20.844	19.312 \pm 0.098	17.135 \pm 0.028
327	21 40 34.60	58 16 37.91	>20.872	18.401 \pm 0.040	16.815 \pm 0.022
331B ^a	21 40 41.32	58 16 37.59	>20.933	16.316 \pm 0.079	14.752 \pm 0.0126
341	21 40 39.32	58 16 40.00	>20.866	18.617 \pm 0.046	17.077 \pm 0.025
357	21 40 40.35	58 16 45.15	>20.895	17.629 \pm 0.019	16.179 \pm 0.013
376	21 40 44.25	58 16 52.37	>20.837	19.563 \pm 0.106	17.099 \pm 0.032
384	21 40 45.30	58 16 53.63	>20.844	19.311 \pm 0.095	16.456 \pm 0.017
388	21 40 46.36	58 16 55.59	>20.850	19.152 \pm 0.074	17.868 \pm 0.057
396	21 40 46.08	58 16 58.88	>20.865	18.635 \pm 0.046	16.825 \pm 0.021
413	21 40 51.15	58 17 01.70	>20.862	18.737 \pm 0.046	17.232 \pm 0.045
414	21 40 51.91	58 17 01.80	>20.868	18.520 \pm 0.041	16.301 \pm 0.021
431	21 40 39.87	58 17 07.23	>20.859	18.839 \pm 0.057	17.489 \pm 0.041
438	21 40 41.78	58 17 08.44	>20.878	18.223 \pm 0.035	17.021 \pm 0.026
460	21 40 43.33	58 17 16.80	>20.868	18.500 \pm 0.037	15.774 \pm 0.008
546	21 40 50.93	58 17 47.55	>20.862	18.753 \pm 0.043	17.884 \pm 0.067
571	21 40 38.64	58 17 55.97	>20.868	18.539 \pm 0.032	17.376 \pm 0.032
627	21 40 33.88	58 18 15.57	>20.850	19.142 \pm 0.064	17.543 \pm 0.035
687	21 40 39.61	58 18 35.16	>20.863	18.690 \pm 0.057	17.014 \pm 0.030
704	21 40 33.39	58 18 43.37	>20.880	18.136 \pm 0.023	17.172 \pm 0.030
747	21 40 36.41	58 18 57.15	>20.851	19.134 \pm 0.083	17.826 \pm 0.048
748	21 40 41.86	58 18 57.35	>20.857	18.905 \pm 0.069	17.113 \pm 0.024
751	21 40 39.28	58 18 58.08	>20.924	16.642 \pm 0.009	15.324 \pm 0.005
762	21 40 51.41	58 19 01.40	>20.883	18.063 \pm 0.059	17.320 \pm 0.045
766	21 40 38.43	58 19 03.16	>20.872	18.443 \pm 0.062	17.658 \pm 0.075
849	21 40 44.67	58 15 05.45	>20.871	18.507 \pm 0.063	18.350 \pm 0.126
853	21 40 47.95	58 15 26.77	>20.850	19.173 \pm 0.099	18.334 \pm 0.115
855	21 40 47.13	58 15 30.18	>20.854	19.050 \pm 0.095	18.057 \pm 0.098
891	21 40 51.53	58 16 09.37	>20.836	19.641 \pm 0.097	18.024 \pm 0.077
896	21 40 47.62	58 16 15.13	>20.850	19.186 \pm 0.080	18.317 \pm 0.104
898	21 40 50.23	58 16 00.27	>20.815	20.360 \pm 0.170	19.320 \pm 0.182
902	21 40 42.07	58 15 29.45	>20.857	18.956 \pm 0.054	18.123 \pm 0.078
904	21 40 38.48	58 15 24.54	>20.866	18.620 \pm 0.042	17.792 \pm 0.078
917	21 40 34.97	58 15 39.58	>20.863	18.721 \pm 0.047	17.373 \pm 0.038
918	21 40 41.90	58 15 21.44	>20.882	18.084 \pm 0.034	17.262 \pm 0.052
920	21 40 40.09	58 15 05.70	>20.846	19.311 \pm 0.088	17.953 \pm 0.076
946	21 40 40.13	58 16 13.92	>20.845	19.340 \pm 0.080	18.550 \pm 0.104
947	21 40 33.19	58 15 57.90	>20.838	19.546 \pm 0.080	17.927 \pm 0.057
948	21 40 40.14	58 16 13.85	>20.845	19.340 \pm 0.080	18.562 \pm 0.107
962	21 40 35.48	58 16 31.40	>20.853	19.055 \pm 0.073	17.526 \pm 0.040
963	21 40 34.76	58 16 19.75	>20.851	19.139 \pm 0.078	18.253 \pm 0.081
964	21 40 32.44	58 16 18.18	>20.854	19.048 \pm 0.058	18.138 \pm 0.071
1024	21 40 49.76	58 16 42.87	>20.845	19.363 \pm 0.082	18.767 \pm 0.142
1025	21 40 48.83	58 16 32.88	>20.830	19.874 \pm 0.148	19.056 \pm 0.167
1029	21 40 49.07	58 16 35.63	>20.834	19.735 \pm 0.125	18.777 \pm 0.137
1031	21 40 52.03	58 16 34.91	>20.845	19.338 \pm 0.089	18.513 \pm 0.129
1033	21 40 50.21	58 16 32.21	>20.826	20.001 \pm 0.142	19.467 \pm 0.241
1057	21 40 49.20	58 16 54.17	>20.842	19.466 \pm 0.094	18.738 \pm 0.136
1059	21 40 52.61	58 17 26.37	>20.845	19.314 \pm 0.105	17.740 \pm 0.079
1061	21 40 48.79	58 17 12.72	>20.856	18.986 \pm 0.060	18.020 \pm 0.079
1062	21 40 49.68	58 17 28.60	>20.836	19.656 \pm 0.102	18.660 \pm 0.127
1067	21 40 42.08	58 16 55.76	>20.844	19.408 \pm 0.105	18.814 \pm 0.142
1070	21 40 39.44	58 17 37.92	>20.829	19.877 \pm 0.188	18.679 \pm 0.131
1075	21 40 34.29	58 16 35.55	>20.825	20.006 \pm 0.159	18.439 \pm 0.098
1076	21 40 33.91	58 16 39.06	>20.832	19.783 \pm 0.126	18.781 \pm 0.132

Table 2. Continued.

NIR source	α (J2000) ($^{\text{h}} \text{ m } \text{s}$)	δ (J2000) ($^{\circ} \text{ } '$ '')	<i>J</i>	<i>H</i> (mag)	<i>K_s</i>
1077	21 40 33.21	58 16 33.94	>20.844	19.366 ± 0.076	18.423 ± 0.101
1078	21 40 34.16	58 17 01.23	>20.841	19.504 ± 0.089	18.960 ± 0.182
1081	21 40 35.10	58 17 02.46	>20.842	19.424 ± 0.099	18.285 ± 0.098
1083	21 40 37.67	58 16 40.27	>20.836	19.622 ± 0.122	17.735 ± 0.045
1085	21 40 34.79	58 16 38.13	>20.850	19.150 ± 0.083	17.617 ± 0.045
1125	21 40 37.87	58 17 19.80	>20.848	19.237 ± 0.087	18.120 ± 0.078
1127	21 40 35.84	58 17 18.85	>20.844	19.401 ± 0.080	18.676 ± 0.139
1129	21 40 41.20	58 17 05.93	>20.829	19.897 ± 0.153	19.160 ± 0.206
1130	21 40 40.44	58 17 06.45	>20.834	19.735 ± 0.119	19.211 ± 0.224
1131	21 40 35.20	58 17 07.97	>20.850	19.194 ± 0.076	18.325 ± 0.107
1141	21 40 31.29	58 16 54.66	>20.830	19.863 ± 0.151	18.984 ± 0.184
1229	21 40 48.94	58 19 01.20	>20.850	19.173 ± 0.128	18.430 ± 0.087
1240	21 40 47.92	58 18 38.12	>20.864	18.701 ± 0.041	17.835 ± 0.053
1242	21 40 52.53	58 18 29.76	>20.868	18.582 ± 0.047	18.043 ± 0.085
1243	21 40 52.67	58 18 24.62	>20.836	19.658 ± 0.144	18.718 ± 0.154
1244	21 40 52.36	58 18 22.13	>20.858	18.908 ± 0.065	18.403 ± 0.123
1248	21 40 48.75	58 18 31.77	>20.843	19.422 ± 0.105	18.632 ± 0.122
1249	21 40 47.79	58 18 27.66	>20.837	19.630 ± 0.102	18.836 ± 0.138
1250	21 40 47.39	58 18 24.04	>20.840	19.528 ± 0.108	18.750 ± 0.126
1251	21 40 47.01	58 18 18.04	>20.846	19.302 ± 0.078	18.507 ± 0.100
1256	21 40 49.98	58 17 58.66	>20.849	19.224 ± 0.081	18.378 ± 0.087
1257	21 40 48.72	58 18 07.72	>20.831	19.834 ± 0.111	18.793 ± 0.119
1261	21 40 46.44	58 18 25.32	>20.853	19.066 ± 0.059	18.286 ± 0.076
1263	21 40 45.46	58 18 18.71	>20.837	19.591 ± 0.086	18.323 ± 0.071
1264	21 40 45.04	58 18 26.24	>20.848	19.248 ± 0.061	18.459 ± 0.096
1265	21 40 44.55	58 18 24.76	>20.855	19.003 ± 0.058	18.029 ± 0.065
1266	21 40 44.28	58 18 35.91	>20.838	19.577 ± 0.095	18.439 ± 0.092
1267	21 40 46.37	58 17 57.89	>20.840	19.531 ± 0.084	18.511 ± 0.112
1269	21 40 44.22	58 18 42.80	>20.845	19.376 ± 0.084	18.782 ± 0.119
1272	21 40 43.26	58 18 52.60	>20.854	19.026 ± 0.067	18.104 ± 0.066
1274	21 40 45.07	58 18 50.80	>20.845	19.361 ± 0.112	18.666 ± 0.110
1275	21 40 44.93	58 18 56.19	>20.857	18.956 ± 0.066	18.261 ± 0.078
1276	21 40 45.25	58 18 58.06	>20.836	19.672 ± 0.153	18.913 ± 0.148
1294	21 40 35.43	58 19 00.83	>20.851	19.155 ± 0.102	18.212 ± 0.071
1299	21 40 34.77	58 18 43.06	>20.849	19.223 ± 0.066	18.401 ± 0.086
1301	21 40 36.11	58 18 36.61	>20.864	18.680 ± 0.039	17.251 ± 0.031
1302	21 40 36.21	58 18 27.49	>20.850	19.169 ± 0.062	18.373 ± 0.089
1309	21 40 38.53	58 17 56.11	>20.860	18.820 ± 0.040	17.635 ± 0.039
1322	21 40 35.28	58 17 52.94	>20.851	19.137 ± 0.064	18.230 ± 0.077
1324	21 40 34.38	58 18 06.24	>20.846	19.277 ± 0.084	17.799 ± 0.065
1332	21 40 31.47	58 18 24.22	>20.839	19.575 ± 0.095	19.120 ± 0.183
1333	21 40 31.76	58 18 24.09	>20.829	19.884 ± 0.115	18.660 ± 0.119
1336	21 40 32.81	58 18 11.29	>20.840	19.510 ± 0.083	18.408 ± 0.098
1338	21 40 33.72	58 18 42.08	>20.857	18.945 ± 0.051	18.107 ± 0.074
1340	21 40 31.97	58 18 45.76	>20.848	19.243 ± 0.072	18.267 ± 0.071
1418	21 40 20.86	58 18 34.97	>20.871	18.490 ± 0.040	17.921 ± 0.073
1428	21 40 31.91	58 17 48.51	>20.823	20.160 ± 0.179	20.281 ± 0.644
1432	21 40 34.55	58 17 53.96	>20.842	19.432 ± 0.087	18.407 ± 0.104
1435	21 40 30.79	58 18 38.65	>20.863	18.770 ± 0.065	18.455 ± 0.079
1443	21 40 32.63	58 18 22.32	>20.830	19.856 ± 0.102	18.848 ± 0.150
1447	21 40 37.54	58 18 23.60	>20.849	19.173 ± 0.079	17.240 ± 0.034
1448	21 40 50.40	58 18 32.59	>20.840	19.534 ± 0.085	18.942 ± 0.095
1449	21 40 46.91	58 17 43.60	>20.853	19.076 ± 0.089	18.264 ± 0.131
1450	21 40 52.64	58 18 09.97	>20.836	19.665 ± 0.127	19.015 ± 0.166
1451	21 40 52.36	58 18 12.48	>20.829	19.874 ± 0.157	18.747 ± 0.130
1452	21 40 51.89	58 17 43.19	>20.808	20.580 ± 0.292	19.127 ± 0.275
1454	21 40 51.61	58 17 45.20	>20.833	19.781 ± 0.125	19.077 ± 0.254
1455	21 40 51.38	58 18 32.81	>20.830	19.860 ± 0.127	18.894 ± 0.178
1476	21 40 31.80	58 17 06.92	>20.840	19.516 ± 0.098	18.718 ± 0.129
1489	21 40 31.67	58 15 45.50	>20.843	19.414 ± 0.089	18.562 ± 0.121
1494	21 40 43.31	58 15 44.45	>20.846	19.328 ± 0.093	18.369 ± 0.095
1495	21 40 43.58	58 15 15.37	>20.852	19.121 ± 0.062	18.299 ± 0.103

(a) The source # 331 is double (see Sect. 3.1). The two components have been labeled A and B. The source # 331A has been detected in the 3 bands and # 331B in the *H* and *K_s* bands only.

Table 3. JHK_s photometry and positions of sources only detected in the K_s band.

NIR source	α (J2000) ($^{\text{h}} \text{ m} \text{ s}$)	δ (J2000) ($^{\circ} \text{ '} \text{ ''}$)	J	H (mag)	K_s
33	21 40 23.31	58 15 04.30	>20.795	>20.086	>19.894
57	21 40 51.67	58 15 11.49	>20.795	>19.869	>14.702
993	21 40 23.88	58 15 09.34	>20.795	>19.933	>16.242
123	21 40 43.52	58 15 26.65	>20.795	>19.997	>17.765
156	21 40 19.80	58 15 36.81	>20.795	>19.996	>16.648
196	21 40 45.77	58 15 49.10	>20.795	>19.993	>17.680
223	21 40 45.17	58 15 59.82	>20.795	>19.922	>15.974
224	21 40 43.45	58 15 59.65	>20.795	>19.924	>16.015
228	21 40 37.58	58 16 01.45	>20.795	>19.980	>17.350
246	21 40 39.61	58 16 09.31	>20.795	>19.927	>16.090
270	21 40 40.16	58 16 18.53	>20.795	>19.962	>16.938
351	21 40 44.59	58 16 42.17	>20.795	>19.963	>16.947
356	21 40 50.02	58 16 44.74	>20.795	>19.997	>17.762
358	21 40 33.84	58 16 45.43	>20.795	>20.011	>18.093
518	21 40 43.57	58 17 34.15	>20.795	>20.004	>17.935
658	21 40 39.82	58 18 25.10	>20.795	>19.972	>17.160
845	21 40 48.68	58 15 17.10	>20.795	>20.039	>18.780
850	21 40 50.13	58 15 40.60	>20.795	>19.999	>17.814
851	21 40 49.35	58 15 36.24	>20.795	>20.021	>18.354
852	21 40 49.23	58 15 38.75	>20.795	>20.032	>18.604
855	21 40 45.66	58 15 44.00	>20.795	>20.013	>18.145
857	21 40 50.48	58 15 27.81	>20.795	>20.053	>19.117
895	21 40 49.07	58 16 10.08	>20.795	>20.052	>19.074
905	21 40 38.61	58 15 26.16	>20.795	>20.013	>18.148
921	21 40 40.28	58 15 08.45	>20.795	>20.019	>18.294
922	21 40 39.22	58 15 10.36	>20.795	>20.030	>18.561
928	21 40 32.86	58 15 17.79	>20.795	>20.053	>19.109
942	21 40 37.16	58 15 59.65	>20.795	>20.012	>18.130
943	21 40 37.49	58 15 43.73	>20.795	>20.036	>18.703
944	21 40 37.74	58 15 38.09	>20.795	>20.036	>18.709
945	21 40 41.72	58 16 12.91	>20.795	>20.000	>17.838
1006	21 40 21.13	58 15 43.47	>20.795	>19.903	>15.510
1022	21 40 52.13	58 16 05.34	>20.795	>20.028	>18.519
1023	21 40 51.80	58 16 08.36	>20.795	>20.038	>18.756
1026	21 40 46.11	58 16 43.49	>20.795	>20.024	>18.415
1028	21 40 48.63	58 16 44.79	>20.795	>20.050	>19.048
1030	21 40 47.64	58 16 34.92	>20.795	>20.048	>18.994
1032	21 40 47.57	58 16 46.33	>20.795	>20.030	>18.569
1058	21 40 50.78	58 16 54.87	>20.795	>20.042	>18.840
1064	21 40 41.17	58 17 18.33	>20.795	>20.020	>18.317
1065	21 40 46.59	58 16 55.50	>20.795	>20.032	>18.618
1066	21 40 42.03	58 16 52.13	>20.795	>20.048	>18.979
1068	21 40 39.77	58 16 59.58	>20.795	>20.033	>18.636
1071	21 40 39.95	58 16 42.41	>20.795	>20.036	>18.702
1072	21 40 41.05	58 16 50.28	>20.795	>20.039	>18.777
1073	21 40 42.30	58 16 46.11	>20.795	>20.042	>18.856
1074	21 40 39.16	58 17 01.60	>20.795	>20.027	>18.486
1079	21 40 34.43	58 16 57.09	>20.795	>20.048	>18.981
1080	21 40 34.75	58 16 57.21	>20.795	>20.107	>20.403
1082	21 40 35.64	58 16 54.81	>20.795	>20.053	>19.116
1128	21 40 36.98	58 17 18.07	>20.795	>20.033	>18.632
1230	21 40 48.60	58 18 59.46	>20.795	>20.021	>18.349
1231	21 40 48.41	58 19 00.59	>20.795	>20.045	>18.912
1236	21 40 48.32	58 18 39.92	>20.795	>20.056	>19.187
1258	21 40 48.68	58 18 09.09	>20.795	>20.057	>19.217
1262	21 40 46.08	58 18 32.35	>20.795	>20.050	>19.037
1268	21 40 41.42	58 18 25.47	>20.795	>20.023	>18.395
1270	21 40 43.06	58 18 43.96	>20.795	>20.009	>18.046
1271	21 40 42.38	58 18 45.49	>20.795	>20.018	>18.260
1289	21 40 39.00	58 18 49.97	>20.795	>20.021	>18.335
1296	21 40 38.31	58 18 41.22	>20.795	>20.021	>18.350
1303	21 40 38.43	58 17 48.85	>20.795	>20.028	>18.501
1304	21 40 37.82	58 17 50.37	>20.795	>20.037	>18.717
1306	21 40 38.18	58 18 08.15	>20.795	>20.025	>18.435
1335	21 40 32.57	58 18 09.04	>20.795	>20.045	>18.917
1337	21 40 36.56	58 18 05.81	>20.795	>20.037	>18.735
1339	21 40 33.99	58 18 52.22	>20.795	>20.022	>18.368

Table 4. JHK_s photometry and positions of sources detected in the J and H bands.

NIR source	α (J2000) ($^{\text{h}} \text{ m} \text{ s}$)	δ (J2000) ($^{\circ} \text{ '} \text{ ''}$)	J	H (mag)	K_s
10000	21 40 19.77	58 15 08.89	18.607 ± 0.063	17.999 ± 0.058	>19.179
10000	21 40 49.57	58 15 08.90	19.882 ± 0.088	18.743 ± 0.047	>19.215
10000	21 40 20.35	58 15 11.71	19.310 ± 0.077	18.618 ± 0.066	>19.210
10000	21 40 21.59	58 15 13.07	19.021 ± 0.042	18.302 ± 0.050	>19.194
10000	21 40 21.91	58 15 14.92	20.409 ± 0.158	19.645 ± 0.169	>19.261
10000	21 40 23.71	58 15 28.66	19.818 ± 0.112	19.147 ± 0.100	>19.237
10000	21 40 27.56	58 15 40.83	20.368 ± 0.137	19.145 ± 0.055	>19.235
10000	21 40 26.72	58 16 00.60	19.986 ± 0.105	19.028 ± 0.055	>19.230
10000	21 40 25.67	58 16 09.40	18.182 ± 0.030	17.914 ± 0.033	>19.176
10000	21 40 23.71	58 16 20.47	20.250 ± 0.126	18.947 ± 0.068	>19.224
10000	21 40 28.48	58 16 25.23	20.406 ± 0.132	19.147 ± 0.053	>19.235
10000	21 40 23.52	58 16 28.54	20.935 ± 0.245	19.837 ± 0.154	>19.270
10000	21 40 30.71	58 16 33.82	18.607 ± 0.036	19.185 ± 0.092	>19.243
10000	21 40 50.17	58 16 46.32	19.292 ± 0.052	18.300 ± 0.033	>19.193
10000	21 40 34.03	58 16 46.81	19.920 ± 0.108	18.947 ± 0.062	>19.226
10000	21 40 28.46	58 16 46.97	18.692 ± 0.050	18.318 ± 0.068	>19.196
10000	21 40 22.40	58 16 52.06	20.362 ± 0.127	19.456 ± 0.113	>19.251
10000	21 40 23.09	58 16 53.49	20.032 ± 0.102	19.043 ± 0.080	>19.230
10000	21 40 39.27	58 16 53.94	19.270 ± 0.059	18.430 ± 0.041	>19.200
10000	21 40 27.30	58 16 55.23	20.213 ± 0.117	19.163 ± 0.065	>19.236
10000	21 40 32.28	58 16 55.48	18.236 ± 0.027	16.995 ± 0.014	>19.127
10000	21 40 22.95	58 17 03.06	20.363 ± 0.135	19.467 ± 0.127	>19.252
10000	21 40 26.72	58 17 05.19	20.024 ± 0.095	19.319 ± 0.074	>19.245
10000	21 40 49.92	58 17 06.42	19.088 ± 0.041	18.362 ± 0.030	>19.197
10000	21 40 27.25	58 17 15.59	19.844 ± 0.078	18.966 ± 0.050	>19.227
10000	21 40 21.50	58 17 16.60	19.868 ± 0.079	19.128 ± 0.080	>19.235
10000	21 40 23.94	58 17 21.90	19.892 ± 0.103	18.766 ± 0.064	>19.216
10000	21 40 23.90	58 17 26.90	19.888 ± 0.131	18.713 ± 0.080	>19.213
10000	21 40 21.07	58 17 32.75	19.984 ± 0.112	18.918 ± 0.091	>19.224
10000	21 40 23.29	58 17 33.73	20.128 ± 0.121	18.846 ± 0.075	>19.219
10000	21 40 21.68	58 17 55.26	20.467 ± 0.137	19.632 ± 0.114	>19.260
10000	21 40 22.07	58 18 01.27	20.064 ± 0.099	19.229 ± 0.093	>19.240
10000	21 40 34.12	58 18 54.05	18.224 ± 0.027	17.720 ± 0.023	>19.165
10000	21 40 33.88	58 15 13.06	19.717 ± 0.069	18.920 ± 0.053	>19.225
10000	21 40 34.23	58 15 08.05	19.536 ± 0.074	18.409 ± 0.038	>19.198
10000	21 40 26.22	58 15 17.62	20.574 ± 0.142	19.295 ± 0.067	>19.242
10000	21 40 23.85	58 15 39.83	20.487 ± 0.170	19.123 ± 0.087	>19.233
10000	21 40 22.74	58 15 19.44	20.374 ± 0.124	19.364 ± 0.106	>19.246
10000	21 40 21.36	58 15 38.50	20.248 ± 0.152	19.003 ± 0.089	>19.227
10000	21 40 23.92	58 15 52.98	20.928 ± 0.186	19.554 ± 0.124	>19.255
10000	21 40 33.11	58 15 23.10	20.367 ± 0.148	19.636 ± 0.101	>19.261
10000	21 40 33.27	58 15 24.85	20.249 ± 0.117	19.507 ± 0.084	>19.254
10000	21 40 31.81	58 15 34.52	20.139 ± 0.106	19.100 ± 0.083	>19.233
10000	21 40 31.15	58 15 36.17	20.473 ± 0.121	19.592 ± 0.086	>19.258
10000	21 40 30.91	58 15 42.31	19.960 ± 0.110	18.760 ± 0.079	>19.215
10000	21 40 27.81	58 15 51.89	20.372 ± 0.136	19.198 ± 0.069	>19.238
10000	21 40 36.14	58 15 21.77	19.743 ± 0.127	18.816 ± 0.102	>19.219
10000	21 40 46.86	58 16 34.34	18.354 ± 0.022	18.827 ± 0.060	>19.224
10000	21 40 36.94	58 16 14.72	19.944 ± 0.121	20.020 ± 0.178	>19.283
10000	21 40 28.07	58 16 36.46	18.865 ± 0.050	18.390 ± 0.039	>19.199
10000	21 40 26.53	58 16 42.88	21.116 ± 0.331	19.471 ± 0.093	>19.250
10000	21 40 25.58	58 16 41.27	20.600 ± 0.191	19.484 ± 0.086	>19.252
10000	21 40 26.09	58 16 06.96	21.167 ± 0.269	19.644 ± 0.092	>19.259
10000	21 40 25.93	58 16 11.34	20.099 ± 0.151	19.245 ± 0.116	>19.241
10000	21 40 22.53	58 16 33.32	18.366 ± 0.028	18.256 ± 0.044	>19.194
10000	21 40 23.31	58 16 38.56	20.410 ± 0.137	19.087 ± 0.068	>19.231
10000	21 40 20.72	58 16 09.81	20.919 ± 0.233	19.483 ± 0.112	>19.251
10000	21 40 19.71	58 16 17.22	19.840 ± 0.191	19.065 ± 0.122	>19.232
10000	21 40 20.46	58 16 18.08	20.205 ± 0.185	19.195 ± 0.111	>19.238
10000	21 40 23.40	58 16 41.82	20.272 ± 0.131	19.526 ± 0.119	>19.255
10000	21 40 27.80	58 17 09.03	20.505 ± 0.147	19.391 ± 0.078	>19.247
10000	21 40 27.70	58 17 13.66	20.830 ± 0.192	19.789 ± 0.108	>19.268
10000	21 40 31.01	58 17 16.59	19.794 ± 0.105	19.691 ± 0.106	>19.266
10000	21 40 33.49	58 17 31.43	20.482 ± 0.184	19.266 ± 0.070	>19.241
10000	21 40 33.73	58 17 06.94	19.340 ± 0.063	18.607 ± 0.045	>19.209
10000	21 40 47.23	58 17 16.28	19.339 ± 0.051	19.266 ± 0.089	>19.245
10000	21 40 47.79	58 17 54.58	20.180 ± 0.129	19.391 ± 0.094	>19.248

Table 4. Continued.

NIR source	α (J2000) ($^{\text{h}} \text{ m} \text{ s}$)	δ (J2000) ($^{\circ} \text{ '} \text{ ''}$)	<i>J</i>	<i>H</i> (mag)	<i>K_s</i>
10000	21 40 26.57	58 17 42.36	20.390 ± 0.191	19.851 ± 0.184	>19.272
10000	21 40 25.71	58 17 42.25	20.969 ± 0.252	19.927 ± 0.145	>19.275
10000	21 40 25.84	58 17 49.89	19.849 ± 0.136	18.949 ± 0.092	>19.226
10000	21 40 24.60	58 17 45.28	20.793 ± 0.202	19.556 ± 0.115	>19.255
10000	21 40 36.40	58 18 47.87	19.999 ± 0.118	19.454 ± 0.135	>19.252
10000	21 40 48.41	58 18 21.10	20.724 ± 0.184	19.995 ± 0.126	>19.279
10000	21 40 21.15	58 15 10.21	20.076 ± 0.106	19.465 ± 0.127	>19.253
10000	21 40 24.14	58 15 35.19	20.013 ± 0.120	19.721 ± 0.156	>19.267
10000	21 40 24.61	58 15 30.92	20.007 ± 0.104	19.478 ± 0.117	>19.254
10000	21 40 22.58	58 15 33.47	20.941 ± 0.296	20.099 ± 0.237	>19.284
10000	21 40 22.46	58 15 39.73	20.338 ± 0.180	19.454 ± 0.134	>19.251
10000	21 40 22.36	58 16 51.10	20.107 ± 0.101	19.429 ± 0.105	>19.251

Table 5. H₂ photometry and positions of the knots.

Knot	α (J2000) ($^{\text{h}} \text{ } ^{\text{m}} \text{ } ^{\text{s}}$)	δ (J2000) ($^{\circ} \text{ } '$ '')	Flux (10^{-15} erg cm $^{-2}$ s $^{-1}$)
HH593A	21 40 44.895	58 16 09.31	7.2519 ± 0.120231
HH593B	21 40 45.030	58 16 08.24	9.7899 ± 0.135257
HH593C	21 40 45.063	58 16 10.18	6.9856 ± 0.122249
HH593D	21 40 45.301	58 16 09.84	9.7167 ± 0.161095
A1	21 40 43.619	58 16 11.47	21.5932 ± 0.278442
A2	21 40 43.630	58 16 09.60	6.3906 ± 0.182471
A3	21 40 43.784	58 16 14.31	7.6761 ± 0.141403
A4	21 40 43.914	58 16 12.88	14.7450 ± 0.203717
A5	21 40 44.124	58 16 15.80	11.4574 ± 0.189955
A6	21 40 44.225	58 16 20.46	6.1969 ± 0.194064
A7	21 40 44.241	58 16 18.11	28.4846 ± 0.314834
A8	21:40:44.425	58:16:14.06	6.2926 ± 0.231835
A9	21 40 44.664	58 16 20.41	8.0101 ± 0.265601
A10	21 40 44.846	58 16 22.90	15.5793 ± 0.243943
A11	21 40 44.887	58 16 19.55	22.6430 ± 0.375402
A12	21 40 45.181	58 16 24.97	22.6024 ± 0.187364
A13	21:40:45.196	58:16:28.04	5.3174 ± 0.142031
A14	21 40 45.386	58 16 22.11	12.7426 ± 0.176052
A15	21 40 45.764	58 16 25.32	44.8619 ± 0.247925
B1	21 40 53.278	58 16 42.45	20.9016 ± 0.365783
B2	21 40 53.690	58 16 42.21	60.9041 ± 0.448773
B3	21 40 54.822	58 16 39.27	19.6719 ± 0.235548
B4	21 40 55.628	58 16 41.07	58.2977 ± 0.375871
B5	21 40 56.159	58 16 42.05	89.9158 ± 0.414091
B6	21 40 56.680	58 16 45.99	31.2816 ± 0.288124
B7	21 40 56.859	58 16 42.94	45.0304 ± 0.248855
B8	21 40 57.290	58 16 42.93	86.4989 ± 0.398356
B9	21 40 57.697	58 16 45.45	7.9630 ± 0.154023
B10	21 40 58.033	58 16 46.92	9.4814 ± 0.259459
B11	21:40:58.147	58:16:48.01	9.2982 ± 0.171284
C1	21 40 38.354	58 18 25.25	2.4505 ± 0.191565
C2	21 40 37.924	58 18 15.25	4.6971 ± 0.110899
C3	21 40 37.708	58 18 23.84	3.9988 ± 0.107372
C4	21 40 37.330	58 18 21.31	4.4350 ± 0.147096
C5	21 40 36.870	58 18 19.05	19.6452 ± 0.117365
C6	21 40 36.507	58 18 18.64	36.7439 ± 0.103129
C7	21 40 36.195	58 18 18.58	49.1595 ± 0.151141
C8	21 40 35.847	58 18 21.68	49.7627 ± 0.169218
C9	21 40 35.830	58 18 15.36	13.6491 ± 0.162850
C10	21 40 35.652	58 18 20.97	40.1287 ± 0.181116
C11	21 40 35.495	58 18 22.55	40.9573 ± 0.213719
C12	21 40 35.220	58 18 20.75	29.1638 ± 0.150897
C13	21 40 35.195	58 18 17.28	45.2751 ± 0.183339
C14	21 40 34.981	58 18 22.25	72.1456 ± 0.147844
C15	21 40 34.801	58 18 23.19	13.3781 ± 0.250208
C16	21 40 34.236	58 18 23.37	51.9956 ± 0.199352
C17	21 40 33.840	58 18 23.79	7.7716 ± 0.161170
D1	21 40 42.454	58 18 39.51	29.4190 ± 0.162581
D2	21 40 42.192	58 18 41.62	23.3558 ± 0.129073
E1	21 40 36.630	58 17 42.06	8.7417 ± 0.193241
E2	21 40 36.360	58 17 39.66	17.9133 ± 0.164993
E3	21 40 36.067	58 17 38.99	42.4345 ± 0.234509
E4	21 40 35.514	58 17 35.21	10.0781 ± 0.213499
F1	21 40 46.190	58 17 40.43	21.9122 ± 0.201826
F2	21 40 45.833	58 17 42.99	19.4522 ± 0.161251
F3	21 40 45.676	58 17 43.53	12.2595 ± 0.124210
F4	21 40 45.151	58 17 47.62	10.6092 ± 0.117261
F5	21 40 44.884	58 17 47.21	28.6625 ± 0.184800
G1	21 40 39.755	58 16 48.88	2.6961 ± 0.079464
G2	21 40 39.638	58 16 50.39	6.3700 ± 0.117343
G3	21 40 39.225	58 16 53.34	19.8301 ± 0.146119
G4	21 40 38.484	58 16 56.81	7.4474 ± 0.144051
G5	21 40 38.143	58 16 58.54	2.4284 ± 0.067100
G7	21 40 37.235	58 17 01.67	4.3884 ± 0.121259
G7	21 40 37.030	58 17 04.44	8.1539 ± 0.180246
H1	21 40 36.305	58 16 21.08	6.0454 ± 0.150342
H2 ^a	21:40:35.750	58:16:10.30	1.7126 ± 0.096224
I1	21:40:39.238	58:16:15.08	1.2868 ± 0.073484
I2	21 40 39.152	58 16 13.63	3.0112 ± 0.116488
I3	21 40 38.813	58 16 16.22	6.8176 ± 0.125589

Table 5. Continued.

Knot	α (J2000) ($^{\text{h}} \text{ } ^{\text{m}} \text{ } ^{\text{s}}$)	δ (J2000) ($^{\circ} \text{ } ' \text{ } ''$)	Flux ($10^{-15} \text{ erg cm}^{-2} \text{ s}^{-1}$)
K1	21 40 41.266	58 16 09.67	17.5391 ± 0.161546
K2	21 40 41.134	58 16 10.60	20.6042 ± 0.132845
K3	21 40 40.335	58 16 06.90	1.9639 ± 0.090445
K4	21 40 40.136	58 16 02.82	12.0642 ± 0.155566
K5	21:40:39.051	58:16:03.05	1.4307 ± 0.084337
L	21 40 42.022	58 16 52.23	2.3914 ± 0.116738
M1	21 40 46.780	58 16 17.13	3.4904 ± 0.083587
M2	21 40 46.831	58 16 16.03	3.1842 ± 0.087986
N1	21:40:47.288	58:16:01.34	2.6871 ± 0.084151
N2	21:40:47.628	58:16:03.70	2.3055 ± 0.084940
N3	21:40:47.939	58:16:02.36	2.5176 ± 0.088116
O1	21 40 53.529	58 17 02.18	6.4074 ± 0.200654
O2 ^a	21 40 55.146	58 16 51.37	3.0039 ± 0.168773
P1	21 40 34.797	58 17 50.74	3.6734 ± 0.115038
P2	21 40 33.721	58 17 54.36	14.2619 ± 0.170770
Q1	21 40 42.436	58 16 00.87	2.1034 ± 0.145301
Q2	21:40:42.351	58:15:57.68	1.6250 ± 0.086812
Q3	21 40 42.256	58 15 55.05	8.2079 ± 0.098280
Q4	21:40:41.586	58:15:52.43	3.2469 ± 0.095700
Q5	21 40 41.327	58 15 54.66	11.3252 ± 0.166899
Q6	21 40 39.844	58 15 45.61	1.3054 ± 0.072144
S1 ^a	21 40 42.377	58 16 14.71	1.3880 ± 0.084378
S2 ^a	21:40:42.748	58:16:22.49	0.8206 ± 0.079362
T ^a	21 40 40.251	58 18 06.11	3.2513 ± 0.101817
U ^a	21:40:41.409	58:16:45.29	0.5961 ± 0.053258
V ^a	21 40 44.378	58 16 50.80	0.8263 ± 0.085241

(a) New detection.